R. & M. No. 3689

MINISTRY OF DEFENCE (PROCUREMENT EXECUTIVE)
AERONAUTICAL RESEARCH COUNCIL
REPORTS AND MEMORANDA

The Measurement of Ground Effect using a Fixed Ground Board in a Wind Tunnel

By L. F. East
Aerodynamics Dept., R.A.E., Bedford

LONDON: HER MAJESTY'S STATIONERY OFFICE
1972
PRICE £2·10 NET

The Measurement of Ground Effect using a Fixed Ground Board in a Wind Tunnel

By L. F. EAST
Aerodynamics Dept., R.A.E., Bedford

Reports and Memoranda No. 3689*
July, 1970

Summary

An experimental and theoretical investigation is made of the method of determining the effect of ground proximity in a wind tunnel using a fixed board to represent the ground. The influence which the boundary layer on the fixed ground board has on the flow about the model has been determined from overall force measurements on three models of aspect ratios 1·6, 3 and 8 and the twodimensional configuration has been solved theoretically. These measurements and calculations show that the boundary layer influence is most significant at the lower aspect ratios and for these configurations an experimental procedure is proposed which enables this influence upon the data to be eliminated. The form of the threedimensional boundary layer which grows on a fixed ground board beneath a low aspect ratio model is discussed and the reason for its influence upon the model explained.

A brief discussion of the form of the threedimensional boundary layer which will grow on a runway as an aircraft passes by is given and the case of infinite aspect ratio (twodimensional flow) has been analysed theoretically.

* Replaces R.A.E. Technical Report 70123—A.R.C. 32 633.

LIST OF CONTENTS

1. *Introduction.*

When an aircraft flies very close to the ground, such as during take-off and landing, the flow about it is modified by the presence of the ground. As a result, the forces acting upon it are changed and in the case of lift this can amount to an increase of as much as 50 per cent for low aspect-ratio wings. This 'ground effect', as the influence of the nearby ground is generally called, is clearly important, but unfortunately its correct simulation in a wind tunnel is difficult.

The simulation in a wind tunnel of an aircraft flying through stationary air relies on the fact that the details of the flow are not changed by any uniform translatory velocity of the whole configuration. Thus the flow about an aircraft in flight is identical to the flow about the same aircraft placed in a uniform flow with a velocity equal and opposite to that of the aircraft in flight. The correct simulation of a fixed ground surface near the aircraft in flight is a surface of infinite extent moving with a velocity equal to the wind tunnel freestream. Naturally this configuration cannot be accurately produced in a wind tunnel and so, by way of introduction to the work described in this Report, the three basic experimental configurations that have been used to approximate to this ideal are now outlined; a more detailed discussion will be found in Ref. 1.

(a) *Moving belt.* The ground-effect configuration can be most closely represented by using a moving belt to represent the ground; such difficulties that do arise are of a practical origin only. The major practical difficulty is obtaining a high belt velocity while at the same time keeping the belt flat: 60 m/s (200 ft/s) would be desirable but the maximum velocity obtainable with the rig described in Ref. 2 is about 27 m/s (90 ft/s). Other difficulties include the rather complex nature of the rig[2, 3] and, if it is mounted in the flow rather than in a wall of the tunnel, its considerable thickness (13 per cent of tunnel height in Ref. 2) which together with the need to keep the rig as short as possible for practical reasons, raises doubts about the uniformity of the flow at the model position because of the curvature of the flow about the leading edge of the rig. In addition, the moving belt, whether it is mounted in the flow or in a wall, can have on its surface a boundary layer formed by the residue of the boundary layer on any fixed surface upstream of the moving belt. Although the displacement thickness of the boundary layer on the moving belt should be small (20 per cent in Ref. 2) compared with the value with the belt stationary, it may still have a significant effect on the flow.

The previous paragraph has touched on some of the many problems associated with turning the moving-belt concept into a practical wind-tunnel tool and it is because of these essentially practical problems that most experimenters have adopted one or other of the two following basic methods.

(b) *Image system.* If two identical models are placed symmetrically about a plane of symmetry of the tunnel working section, then in theory, the plane of symmetry will be a stream surface and so can be treated as a plane ground surface. This configuration represents the 'inviscid' ground effect as the boundary layer which will develop on the ground as an aircraft passes by will not be represented. The experimental rig[1, 4] is complicated and the scale of the models has to be significantly reduced, but the main difficulty with the technique arises from doubts about the spacial stability of the vortices shed from the two models which, if they are not exactly matched or have any tendency to coalesce, will result in the geometric plane of symmetry not being a stream surface. This interaction between the vortices can be eliminated by inserting a splitter plate[4] on the plane of symmetry and between the model wakes. The required upstream extension of this splitter plate would need to be determined by experiment for any particular aircraft configuration and the plate itself must be sufficiently thin for its displacement not to affect the model flow significantly.

(c) *Fixed ground board.* The most common method of representing the ground is to use a fixed board[5, 6, 7] or a surface of the tunnel working section. This requires a relatively simple experimental rig but has the major drawback that a boundary layer inevitably grows on the board. Various methods have been used to reduce the boundary layer and hence, by inference, its effect on the flow. The most obvious means of thinning the boundary layer beneath the model position is simply to reduce the upstream extension of the ground board. There comes a point in this process at which the flow at the leading edge of the ground board is significantly affected by the pressure field of the model and further reductions of the length of the ground board will cause errors due to the ground not being fully represented. Further reductions of the length of the ground board are made possible by placing a second, similar, but not necessarily identical, model on the opposite side of the ground board from the test model. The purpose of the second model

is to straighten out the attachment line on the leading edge of the ground board and the upstream flow by imposing a threedimensional pressure field in this region to balance that of the test model. Although this arrangement appears similar to the image system with splitter-plate arrangement mentioned above, they differ fundamentally in that the ground is represented in the former by a ground board with a second model, which need be only roughly similar to the test model, to correct the details of the upstream flow, whereas it is represented in the latter by the flow induced by the second identical model with the addition of a splitter plate, which only serves to stabilize and correct the details of the downstream flow. The boundary layer may also be thinned by suction or slots which remove low energy fluid from the layer. The difficulty with these methods is that the removal of fluid is likely to cause significant and unknown flow disturbances at the model position.

Generally, whatever modifications are made to the basic fixed ground board rig there will still be a boundary layer beneath the model position and the penalties for such modifications are added experimental complexity and additional uncertainties about the flow. It has accordingly been the practice at R.A.E. to use a plain fixed board for all ground-effect tests except when the moving belt is used with models which would cause excessive interaction between the model and the boundary layer on a fixed board (e.g. V/STOL models)[3]. However, recent unpublished tests[7,8,9] have raised doubts about the accuracy obtained with a fixed board and the work described in this Report was undertaken to account for the discrepancies that have arisen and to obtain a clearer understanding of the effects of the boundary layer, which grows on the ground board, upon the flow about the model. The largest effects may be expected when the adverse pressure gradients caused by the model are sufficient to separate the boundary layer, but under these circumstances the flow does not even approximate to the true ground effect configuration and no reliance should be placed on measurements obtained. This Report is concerned with less severe conditions in which the boundary layer remains attached throughout the length of the ground board.

The first objective of this Report is to determine whether the boundary layer on a fixed ground board is a sufficient source of error to account for the discrepancies between past measurements and, if so, the second objective is to propose and investigate methods of obtaining more accurate ground effect results from the standard fixed ground-board rig. The basis of the method proposed for reaching these objectives is described in the following section and the experimental and theoretical investigations made are described in sections 3 and 4.

2. *Basis of the Investigation.*

The most straightforward approach to the problem of reaching the objectives described above, would be to calculate the effect of the boundary layer on the ground board theoretically. Although feasible in two dimensions (*see* Section 4) this would be a formidable computation in three dimensions, since it involves using a detailed representation of the threedimensional model in its high lift configuration, computing the threedimensional development of the boundary layer on the ground board and then computing the detailed effects of the boundary layer on the model. The correct solution would then be found by iteration.

An alternative approach, which is now outlined, is used in this Report. At a given flow Reynolds number and Mach number the detailed flow about a model close to a fixed ground board is uniquely defined by the geometries of the model, the ground board and the enclosing wind tunnel together with their relative positions. Consequently for a fixed model attitude at a fixed height above the ground board, the flow about the model is only a function of the upstream extension of the ground board (L) providing the ground board is a simple flat plate and that it extends sufficiently far downstream of the model position for variations of the trailing-edge position to be unimportant. Thus if ϕ is any characteristic of the flow about the model, such as lift coefficient or static pressure at a particular point on the model surface,

$$\phi = \phi(L). \tag{1}$$

Providing the ground board length (L) is not so short that the flow around its leading edge is significantly affected by the pressure field of the model, which would imply that even in the absence of boundary layers the potential flow would not represent the full ground effect, then the ground board length will only affect the flow about the model indirectly as a result of the ground board's boundary layer. In general, in the

presence of the model, this boundary layer will be threedimensional but nevertheless its influence upon the external flow will be the same as a distribution of displacement thickness over the surface of the ground board. Since the distribution of displacement thickness in the presence of the model is a single valued function of the ground board length (L) and the displacement thickness beneath the model position in the absence of the model is a monotonic function of L, then the former is also a single valued function of the latter. Consequently the displacement thickness of the boundary layer on the ground board beneath the model's position, measured in the absence of the model (δ^*), can be used as the independent variable in place of L in equation (1). Thus,

$$\phi = \phi(\delta^*). \tag{2}$$

A corrected value of ϕ can therefore be obtained by extrapolating to $\delta^* = 0$ but, as discussed in greater detail in Section 3.3, this process does not eliminate the effects of the growth of the ground-board boundary layer since $\partial\delta^*/\partial x$ and $\partial^2\delta^*/\partial x^2$ do not tend to zero as δ^* tends to zero. The effect of the slope of the displacement surface ($\partial\delta^*/\partial x$) on the model flow will be small but significant (Section 3.3) and the effect of the curvature ($\partial^2\delta^*/\partial x^2$) will be extremely small and can be ignored. Consequently equation (2) is written in the form,

$$\phi = \phi(\delta^*/h, \partial\delta^*/\partial x), \tag{3}$$

which, to first order in δ^*/h and $\partial\delta^*/\partial x$, can be extrapolated to $\phi(0,0)$ using the equation,

$$\phi(0,0) = \phi(\delta^*/h, \partial\delta^*/\partial x) - (\delta^*/h)\,\partial\phi/\partial(\delta^*/h) - (\partial\delta^*/\partial x)\,\partial\phi/\partial(\partial\delta^*/\partial x). \tag{4}$$

The last term in equation (4) represents an induced incidence which can be estimated from the measurements of ϕ as a function of incidence (α) and which in general will be small and will vary very little with δ^*/h (*see* Section 3.3). Since the last term varies very little with δ^*/h equation (4) simply states that any function of the model flow plotted against (δ^*/h) should yield a linear relationship. The estimate of the true ground effect obtained by correcting for $\partial\delta^*/\partial x$ and extrapolating to zero δ^*/h will represent the 'inviscid' ground effect but may still be in significant error as the effect of the boundary layer which will grow on a runway under the influence of the induced flow of the aircraft is not represented. This aspect is considered further in Sections 4, 6 and Appendix III.

Equation (4) forms the basis of the method proposed in this Report for determining more accurately the effect of ground proximity and the experiments undertaken were aimed at verifying its applicability and determining some of its limitations.

3. *Wind Tunnel Tests.*

3.1. *Details of Tests.*

This section describes a series of wind tunnel tests which were designed to achieve the two objectives given in Section 1. In order to demonstrate the dependence of the flow about a model upon δ^* it was necessary to vary δ^* independently of L and this was done by artificially thickening the boundary layer to two different extents for each ground board length. This produced three different values of δ^* for each value of L and, as three ground board lengths were used, nine different configurations were obtained. The velocity profiles measured on the ground board beneath the model position with the model removed are plotted in Fig. 1. The profiles show that the thickened boundary layers had not returned to equilibrium 'flat plate' layers and this could be a cause of spurious 'second order' effects, since strict similarity has not been retained while varying δ^* and L independently (*see* Section 3.2).

The general arrangement of the ground board and model in the wind tunnel working section is shown in Fig. 2. The models were suspended from an overhead lever-balance by wires which passed through small holes in the ground board. The holes were generally not more than about 0·001 m^2 (1·5 in^2) although previous tests had shown that the holes did not really need to be so small as appreciably larger holes did

not produce measurable effects[8]. The downstream extension of the ground board was not changed throughout the test. Details of the calibration procedure used with the ground board in position are given in Appendix I. Special care had to be given to calibration for these tests to be meaningful and the calibration procedure described was carried out for each of the nine combinations of L and δ^*.

Three different models were tested. Model 1 was a thin slender delta of aspect ratio 1·616 and its planform is shown in Fig. 3 together with leading dimensions. This model is similar, but not identical, to that used by Kirkpatrick[6] in his detailed experiments on ground effect. Model 2 (shown in Fig. 4) was a symmetrical wing of aspect ratio 3 and 45 degrees sweepback. This model has been previously used by Küchemann, Weber and Brebner[10] for force and pressure measurements and by Brebner[11] for boundary layer measurements. Model 3 (shown in Fig. 5) had a swept and tapered wing of aspect ratio 8 together with a large diameter fuselage. The wing was set in the fuselage at a positive incidence of 4 degrees and with the trailing edge of the root chord half a radius below the fuselage centre line. Previous tests with this model are unpublished[12] apart from the results given by Lovell[13] which refer to the same wing but a different fuselage.

Each of the three models was tested in close proximity to the ground board using each of the nine combinations of δ^* and L. Lift, drag and pitching moment were measured for a range of model incidence. The nominal flow velocity used throughout was 61 m/s (200 ft/s) and transition was not fixed on any of the models.

3.2. *Experimental Results.*

The measured data have been reduced to coefficients using the appropriate calibration for each ground board configuration. No additional blockage, constraint or wire drag correction has been applied as these will be constant for a given model attitude and ground height and so will not affect the relationship between measurements obtained with different ground board boundary layers.

The complete set of data is given in Figs. 6–17. In addition to the lift coefficient C_L, the drag coefficient C_D and the pitching moment coefficient C_M measured about the pitch axes specified in Figs. 3–5, the position of the centre of pressure $(\bar{x}/c)$ is also presented. These functions are plotted against (δ^*/h) and data obtained from different ground board lengths (L) are distinguished by different symbols. Figs. 6–17 show that the functions (C_L etc.) vary appreciably with (δ^*/h) and so the first objective is reached. The very small amount of scatter about the mean curves indicates that the effects of ground board length and of the variations of the shape of the boundary layer profiles which occur as a result of boundary layer thickening (Section 3.1) are either individually negligible or, if significant, cancel each other out. It seems implausible that such a cancellation of effects should occur so consistently for so wide a range of conditions and it is therefore concluded that neither L nor the shape of the boundary layer profile has a significant independent effect upon the flow about the model and that consequently δ^* is the correct independent variable.

The second objective, which was reduced in Section 2 to showing whether equation (4) can be used to correct experimental data, can also be investigated using Figs. 6–17. According to equation (4) the variation of any flow characteristic (C_L etc.) with (δ^*/h) should be linear, provided that the $\partial\delta^*/\partial x$ term in equation (4) does not vary much with δ^*/h, and a glance at Figs. 6–17 will show that in most cases the variations are linear. The straight lines shown on Figs. 6–17 have the least value of the mean of the squares of the deviations. In making this calculation the deviations have been weighted by the inverse of (δ^*/h) and so are weighted in favour of the experimental points obtained at the lower values of (δ^*/h).

Considering Figs. 6–17 in greater detail it is seen that the experimental points obtained with the slender delta (Figs. 6–9) lie close to the straight lines shown and that an accurate extrapolation to $\delta^*/h = 0$ is possible. The reason for plotting $\bar{x}/c$ in addition to C_M is that variations of the pitching moment about a fixed point necessarily include variations of C_L and C_D, and the slopes of curves of C_M against (δ^*/h) are therefore dependent upon the position chosen for the pitch axis. This difficulty can be overcome by using the position of the centre of pressure $(\bar{x}/c)$ together with the two components of that force (C_L and C_D) which then show the effects of the ground board's boundary layer much more clearly. This, of course, is not true when C_L is small and C_M relatively large but this is not a situation of practical interest in the vicinity of the ground, when large lift coefficients are required.

The results for Model 2, shown in Figs. 10–13, also show a reasonably linear behaviour though the variations of C_L with (δ^*/h) are appreciably less than for Model 1. Significant non-linearities are evident at the highest incidence, $\alpha = 16$ degrees, and this is probably attributable to the wing tips which extended well into the ground board's boundary layer and so significant higher order effects are to be expected. In the analysis that follows in Section 3.3 the data relating to Model 2 at an incidence of 16 degrees have been omitted. The inconsistent values of C_M and $\bar{x}/c$ at $\delta^*/h = 0{\cdot}045$ probably result from an experimental error being made in the setting up of the pitching moment zero.

The results for Model 3 (Figs. 14–17) show that the dependency of the flow upon (δ^*/h) is less than for Models 1 and 2, and is also markedly non-linear. Thus the second objective has been reached insofar as it has been shown that equation (4) forms a satisfactory means of correcting the data from the low-aspect-ratio models (1 and 2) but not from the high-aspect-ratio Model 3.

As the ordinates of Figs. 6–17 have false origins, the significance of the variations of the coefficients with (δ^*/h) is obscured. Figs. 18–20 show the variation of lift coefficient with incidence for the three models. The free air lift coefficients are shown together with estimates using the straight lines on Figs. 6–17 for the models near the ground board with $\delta^*/h = 0$ and 0·05. These figures show that the apparent error ranges from about 10 per cent of the free air C_L for Model 1 down to about 2 per cent for Model 3 and that the ground effect itself ranges from about 50 per cent for Model 1 down to about 5 per cent for Model 3.

3.3. *Analysis of Results.*

The data presented in Section 3.2 have demonstrated that measurements of ground effect made with a fixed ground board can be in significant error. The data have also shown that, for the two models with the lowest aspect ratios, the error is proportional to δ^* for a particular model attitude and ground height. No general solution for calculating the constants of proportionality $(\partial\phi/\partial(\delta^*/h)$ in equation (4)) can be given, but for the special cases when ϕ represents C_L, C_D and $\bar{x}/c$ the functional dependence of $(\partial\phi/\partial(\delta^*/h))$ has been deduced by a simple analysis in Appendix II.

The analysis includes various simplifying assumptions and is designed solely to provide a basis for the correlations of the experimental data given in this section. It is based upon a concept of the flow, which is described in detail in Section 5 and which assumes that the predominate interaction between low-aspect-ratio models and the ground board boundary layer is caused by the divergence of the boundary layer induced by the flow field of the model.

The equations given in Appendix II only represent the lift-induced part of $(\partial\phi/\partial(\delta^*/h))$ and so to make comparisons with the data the zero-lift component has been subtracted from the data. This zero-lift component is due primarily to the thickness and camber of the wing and the growth of the ground board boundary layer due to viscous effects. Subtracting the zero lift component implies that these secondary effects are independent of incidence and although this will not be generally true it is an adequate assumption for the present purposes since these effects are small compared with the direct lift effect. A more detailed consideration of the effect of the growth of the ground board boundary layer is given later in this section.

Equation (B.13) gives the dependence of the lift coefficient upon δ^* and for comparison with the data is written in the form,

$$\left(\frac{\partial C_L}{\partial(\delta^*/h)}\right) - \left(\frac{\partial C_L}{\partial(\delta^*/h)}\right)_{C_L = 0} = K_1(C_L\, c/h)\left(\frac{\partial C_L}{\partial \alpha}\right). \tag{5}$$

Fig. 21 shows that this equation correlates the data from Models 1 and 2 very closely and yields a value of K_1 of $-0{\cdot}09$. The data from Model 3 has not been included in Fig. 21 for, as will be seen on Fig. 14. the variation of C_L with (δ^*/h) shows appreciable scatter as well as curvature. Virtually all the scatter has been removed on Fig. 22 by plotting $\Delta C_L = C_L - (C_L)_{\alpha = -4^\circ}$ against (δ^*/h). As the zero-lift condition has not been measured for Model 3, comparisons with the analysis are best made using some other model attitude as a datum and for this purpose the lowest incidence (-4 degrees) for which measurements were

made, has been used. The slopes of the straight lines in Fig. 22 were calculated using equation (5) written in the form,

$$\left(\frac{\partial C_L}{\partial(\delta^*/h)}\right)-\left(\frac{\partial C_L}{\partial(\delta^*/h)}\right)_{\alpha=-4^\circ}=K_1\left(C_L\frac{\partial C_L}{\partial\alpha}-\left(C_L\frac{\partial C_L}{\partial\alpha}\right)_{\alpha=-4^\circ}\right)(c/h) \tag{6}$$

and the slopes appear to be of the right order.

Equation (B.14) gives the dependence of the drag coefficient upon δ^* and can be written in the form,

$$\left(\frac{\partial C_D}{\partial(\delta^*/h)}\right)-\left(\frac{\partial C_D}{\partial(\delta^*/h)}\right)_{C_L=0}=K_1(C_L\,c/h)\left(\frac{\partial C_D}{\partial\alpha}-C_L\right). \tag{7}$$

Using the value of K_1 of $-0{\cdot}09$ deduced above, Fig. 23 shows that the data lie close to the line given by equation (7) for Model 1. The experimental values of $(\partial C_D/\partial(\delta^*/h))$ for Model 2 are very much smaller than for Model 1 and, as shown in Fig. 24, this is predicted by equation (7). The low values result from the two terms in $(\partial C_D/\partial\alpha - C_L)$ being approximately equal and although this results in low accuracy, the general trend of the data (Fig. 24) is followed by the calculated points. By writing equation (7) in a similar form to equation (6) the value of $(\partial(\Delta C_D)/\partial(\delta^*/h))$ can be calculated for Model 3 ($\Delta C_D = C_D-(C_D)_{\alpha=-4^\circ}$). The lines in Fig. 25 have slopes calculated in this way and although the slopes are rather large they are of the right order and of the correct sign, which is opposite to the sign of $(\partial C_D/\partial(\delta^*/h))$ for Model 1.

The variation of the position of the centre of pressure is given by equation (B.16) as,

$$\frac{\partial(\bar{x}/c)}{\partial(\delta^*/h)}=K_2(c/h) \tag{8}$$

which, it will be noted, requires that the gradients of the curves shown in Figs. 9, 13 and 17 should be the same for any particular model at the higher incidences. This is clearly so for Model 1 (Fig. 9) but not for Model 2 (Fig. 13) while the variation of $\bar{x}/c$ with δ^*/h for Model 3 is so small as to preclude any definite conclusion.

The correlations made in this section have demonstrated the coherence of the effect of the boundary layer on a fixed ground board, upon the lift and drag of models of different aspect ratios and widely differing shapes. Although the equations developed should not be used to correct experimental data, since other variables such as Reynolds number are likely to have significant effects, they could be used to estimate the likely order of errors in data obtained with a fixed ground board.

Hitherto the correction for the viscous growth of the ground board boundary layer which is approximated by the last term in equation (4) has not been evaluated. The need for this term will depend upon the behaviour and influence of the gradient $\partial\delta^*/\partial x$ and the curvature $\partial^2\delta^*/\partial x^2$ of the boundary layer as δ^* is reduced to zero. If both $\partial\delta^*/\partial x$ and $\partial^2\delta^*/\partial x^2$ tend to zero as δ^* tends to zero then no correction is required and in principle such data could be obtained by using a moving belt rig at various speeds below the freestream velocity. If, however, $\partial\delta^*/\partial x$ and $\partial^2\delta^*/\partial x^2$ do not tend to zero as δ^* tends to zero, as is the case with a flat-plate boundary layer, then the additional correction is required. In practice ground boards are relatively long and the growth of the boundary layer due to viscous effects is small. Since the model height is small compared with the ground board length the correction will be equivalent to an induced incidence of $-\partial\delta^*/\partial x$ and an induced curvature of the flow of $-\partial^2\delta^*/\partial x^2$, though the latter can be ignored as being negligible compared with the former. Strictly this correction should be applied to the data before an extrapolation to $\delta^* = 0$ is made, but in practice the variation of the induced incidence may be sufficiently small over the experimental range of δ^* for an accurate result to be obtained by extrapolating the data to $\delta^* = 0$ and then applying the extrapolated induced incidence correction. For the present data, which covers a wide range of δ^*, the estimated induced incidence, assuming flat plate boundary layer development, varies from 0·15 degrees at $\delta^* = 3{\cdot}9$ mm (0·15 in) to 0·11 degrees at $\delta^* = 13{\cdot}4$ mm (0·53 in). Hence

the data which has been obtained by extrapolation to $\delta^* = 0$ could be corrected for an extrapolated value of the induced incidence of, say, 0·16 degrees.

The data of Model 1 have been corrected in this way and are shown in Figs. 26 and 27. The effects on lift and drag are small but significant, while the effect on $\bar{x}/c$ is minute for the higher incidences and is therefore not shown.

The above procedure should yield the 'inviscid' value of the ground effect. That is the value that would occur if the fluid passing over the ground board or the fluid in the vicinity of a runway were inviscid. The true ground effect will include the boundary layer on the runway induced by the flow field of the aircraft passing overhead. This additional effect, which would be reproduced by a perfect moving belt rig, is discussed in Section 6.

4. *Twodimensional Analysis.*

An analysis of the forces on a twodimensional lifting aerofoil positioned near a fixed ground board was undertaken to complement the threedimensional wind tunnel tests described in Section 3. The method used involved solving the inviscid flow about the aerofoil, its image and a third body having the shape of the displacement thickness of the boundary layer on the ground board using the Smith and Hess[14] computed program and calculating the boundary layer on the ground using the entrainment method of Head[15]. It was found that the influence of the boundary layer on the ground board on the local freestream flow was such as to require several iterations before the boundary layer and the freestream were compatible. As each iteration included a three-body solution of the Smith and Hess program this made the solution excessively expensive. Further it was found that the influence of the ground board's boundary layer upon the lift of the aerofoil was small and so only a very limited set of solutions has been obtained. These are given in Fig. 28 and refer to an N.P.L. 'A' (HSA 681 'A') section aerofoil with a 10 degree droop of the leading 15 per cent chord and 10 degree deflection of the trailing 30 per cent chord. The angle of incidence is 5 degrees giving a free air lift coefficient of 1·573 and the results are for the two ground heights of $h/c = 0{\cdot}5$ and 1·0. Fig. 28 shows the fractional change of the lift coefficient relative to the 'inviscid' value as a function of δ^*/h. It is shown that the change in the value of C_L is small and that for neither ground height do the uncorrected values of ΔC_L extrapolate to zero as δ^* tends to zero. The circular and triangular symbols in Fig. 28 show two methods of correcting for the growth of the boundary layer in the absence of the aerofoil. The circles are corrected, as in Section 3, simply for an induced incidence of $\partial\delta^*/\partial x$ while the triangles have been corrected by calculating the effect of the flat plate boundary layer using the Smith and Hess program. On the sensitive scales of Fig. 28 both corrections are large and the difference between them is smaller but still significant. At the lower ground height ($h/c = 0{\cdot}5$) the corrected values of ΔC_L clearly extrapolate more nearly to zero as δ^* tends to zero while with the higher ground height ($h/c = 1{\cdot}0$) ΔC_L appears to be virtually zero and the extrapolation depends upon the correction used. It is tentatively concluded from these curves that a correction for the flat plate boundary layer should be applied and that providing δ^*/h is not too small (say $\delta^*/h > 0{\cdot}01$) an incidence correction of $\partial\delta^*/\partial x$ is adequate. This supports the procedure previously adopted in Sections 2 and 3.

The effect of the boundary layer which would grow on a fixed surface as the twodimensional aerofoil passed by, is shown in Fig. 28 by the square symbols at $\delta^*/h = 0$. Since this configuration includes the true ground boundary layer it represents the true ground effect of practical interest, but, as shown in Fig. 28, the calculated lift coefficient differs insignificantly from the inviscid solution ($\Delta C_L \leqslant 0{\cdot}05$ per cent C_L) for the two cases computed. The method used to compute the displacement thickness of the true ground boundary layer is described in Appendix III. It represents an extension of the entrainment method to an application for which there is no experimental information and consequently the accuracy of the calculated development is uncertain. The development of δ^* calculated for the two configurations used in Fig. 28 is given in Fig. 29, which shows that δ^* is negative throughout and reaches a minimum beneath the aerofoil. About one chord downstream of the trailing edge, separation is predicted which corresponds to the separation profile sketched in Fig. 30. The calculation method can go no further downstream and the curves have therefore been extrapolated to zero δ^* far downstream, ignoring the last couple of computed points which are probably in error. Thus, although the numerical accuracy of the boundary layer calculation is unknown, the solutions obtained follow the expected forms (*see* Appendix III) and the displacement

thickness is so extremely small that it may safely be concluded that for twodimensional aerofoils the influence of the true ground boundary layer on the flow about the aerofoil is insignificant.

5. *The Boundary Layer on a Fixed Ground Board.*

The results obtained in Sections 3 and 4 indicate that there must be significant differences between the characteristics of the boundary layer on the fixed ground board beneath twodimensional and three-dimensional models. For in Section 4 it was shown that the effect of the ground board boundary layer on the twodimensional aerofoil was very small and markedly non-linear, while in Section 3 it was found that for models of low aspect ratio the effects were large, linear and, so far as lift and drag are concerned, could be represented by an induced incidence.

Typical displacement surfaces calculated in the twodimensional study are shown in Fig. 31 and show that the boundary layer thickness increases rapidly upstream of the aerofoil in the adverse pressure gradient induced by the circulation of the aerofoil and its image. The critical region of the boundary layer development, insofar as it affects the aerofoil, is beneath the aerofoil itself. Here the passage between the lower surface of the aerofoil and the ground board forms a twodimensional duct in which the pressure gradients are largely due to the slope and position of the lower surface of the aerofoil and the displacement surface of the ground board boundary layer itself. Downstream of the trailing edge of the aerofoil the pressure gradient is favourable and the boundary layer is initially thinned. Clearly the actual shape that the boundary layer displacement surface assumes is dependent upon a number of details of the configuration and there is no controlling influence giving rise to an overall slope of the displacement surface.

Fig. 32 shows the streamline pattern obtained by using the oil flow visualisation technique on the ground board beneath Model 1. The strong divergence of the flow is evident and it is this divergence which is considered to be the cause of the relatively large effect that the ground board boundary layer has on the forces acting upon the low-aspect-ratio models. For all practical wing shapes the flow induced near the ground board by the wing and its image in the ground plane will be directed away from the centre line of the configuration over the whole ground plane*. Fig. 33 shows a sketch of a possible centre line section through a steadily diverging flow of the type shown in Fig. 32. The sketch shows that the thickness of the boundary layer probably does not change rapidly (the boundary layer does not for instance vanish downstream) and the action of the divergent flow is to progressively reduce the displacement thickness, which in all probability becomes negative (as shown in Fig. 33). The inviscid part of the flow can be calculated by adding the displacement thickness to the ground board surface to obtain the displacement surface and then solving the potential flow about this surface and the model. The part of the potential flow which is outside the physical boundary layer is the required flow solution while the remainder of the solution, that is within the boundary layer and through the ground board surface, is equivalent to the sink-effect of the boundary layer produced by the lateral movement of the low energy air. To either side of the model the flow will be convergent (Fig. 32) and the boundary layer will pile up, producing a progressively greater displacement thickness. Thus the action of the low aspect ratio wing on the boundary layer is rather akin to that of a snow plough but with the additional feature that the thinning of the boundary layer in the path of the model and the thickening to either side, will continue downstream under the influence of the trailing vorticity. This latter fact is the cause of the well known corrugated boundary layer to be found downstream of a row of vortex generators.

The simple analysis given in Appendix II is based on the concept of the flow discussed in this section and it is evident that if the section through the flow sketched in Fig. 33 is substantially correct, then the influence of the boundary layer upon the model could be large and also equivalent to an induced incidence.

6. *The True Ground Boundary Layer.*

It is generally assumed that the boundary layer induced on a runway by an aircraft passing by has a negligible effect upon the aircraft. For the twodimensional cases calculated in Section 4, the effect of the true ground boundary layer was shown to be a negligibly small reduction of lift. In principle a similar

* The only exception to this generalisation would be a wing with a large angle of forward sweep which might induce a flow towards the centre line over a part of the ground plane.

analysis of the threedimensional boundary layer could be made for a given pressure field using an extended form of the entrainment method but as this has not been done, the probable form that the boundary layer will take is now discussed.

Considering the threedimensional configuration in axes fixed in the model and hence with the ground moving with the undisturbed freestream velocity, it is clear that the velocity of the air in the boundary layer will be greater than the local freestream velocity but less than the moving ground velocity. Consequently the divergence of the air in the boundary layer will be less than the divergence of the local freestream and in the limit, as the ground is approached, will tend to parallel flow (cf. the flow over a fixed ground board). Therefore the diverging freestream will cause the displacement thickness of the boundary layer beneath the wing to increase and consequently result in a positive induced incidence at the model. The magnitude of this induced incidence is not known but it is expected to be appreciably less than is induced by the fixed ground board because the boundary layer thickness (not displacement thickness) will be much less, as was shown in the twodimensional study. The magnitude will however be more than in the twodimensional flow, if the assumption that the divergence of the flow is the controlling influence, is valid.

It is concluded that the effect of the true ground boundary layer on a low aspect ratio wing will be equivalent to a positive induced incidence of magnitude greater than in the twodimensional flow but less than is caused by a fixed ground board. Whether this effect will be significant remains uncertain.

7. *Experimental Procedure for Obtaining Ground Effect Measurements Using a Fixed Ground Board.* The following procedure is suggested :—

(a) Select at least two ground board configurations which will provide widely spaced values of the displacement thickness of the boundary layer at the model position. The configurations may differ in the upstream extension of the ground board or by the addition of devices near the leading edge of the ground board to thicken the boundary layer.

(b) Calibrate each of the ground board configurations using the method set out in Appendix I and, at the same time, measure the boundary layer profile at the model position. The gradient of the boundary layer displacement thickness at the model position can also be measured but a calculation using a normal flat-plate relationship will probably give this gradient with sufficient accuracy.

(c) Install the model in the tunnel and repeat all the required measurements for each ground board configuration. Ensure that for every measurement made the static pressure, as recorded by the reference probe (Fig. 2), is noted.

(d) Reduce the raw data to the appropriate nondimensional form using the calibrations of sub-section (b) and the static pressures measured in sub-section (c).

(e) Linearly extrapolate the reduced data to zero boundary layer displacement thickness using the values of displacement thickness deduced from the measurements made in sub-section (b).

(f) Finally apply an induced incidence correction obtained by linearly extrapolating either the measured or the calculated values of the gradient of the displacement thickness to zero displacement thickness.

In addition to the above procedure it would be good practice to confirm by flow visualisation that the ground board boundary layer does not separate under the most severe conditions being tested. Also, when testing high aspect ratio wings, the procedure may fail owing to non-linearities for which a particular look-out should be kept, though this will, of course, require measurements from more than two ground board configurations.

The above procedure is designed to correct for the effects of the boundary layer on the fixed ground board, and additional corrections should be applied for tunnel blockage and constraint, and for wire drag.

8. *Conclusions.*

This Report is concerned with the experimental technique of simulating in a wind tunnel the flow about an aircraft flying close to the ground, by representing the ground by a fixed surface in the moving tunnel flow. It has been demonstrated that the results obtained vary according to the thickness of the boundary layer which grows on the fixed surface. The influence of the boundary layer is most significant on low aspect ratio models, for which the ground effect itself is also greatest, and it is shown to be equivalent to an induced incidence. The induced incidence is proportional to the displacement thickness of the two-

dimensional boundary layer that exists on the ground board beneath the model position, when the model is removed. This fact enables an experimental technique to be established which yields corrected data. The relatively large influence that the threedimensional boundary layer on the ground board has on the model is explained by the divergence of the flow beneath and downstream of the model which progressively reduces the effective displacement thickness of the boundary layer.

A twodimensional analysis of the growth of the boundary layer which grows on a runway as an aircraft passes by has shown it to be very thin and to have a negligible effect upon the twodimensional wing. It is argued, however that this boundary layer will have a larger effect upon the low-aspect-ratio wings, but as it has not been quantified, the significance of this effect remains unknown.

LIST OF SYMBOLS

A	Cross-sectional area
C_D	Drag coefficient
C_f	Skin friction coefficient, $C_f = \tau_o/\frac{1}{2}\rho\, u_e^2$
C_L	Lift coefficient
C_M	Pitching moment about pitch axes (Figs. 3–5)
c	Mean chord of wing
h	Height of model above ground board (experimentally, height of pivot axis above ground board)
H, H_1, H', H_1'	See Fig. 34 for definitions
K_1, K_2	Constants introduced in equations (B.13) and (B.16)
L	Upstream extension of ground board from model position (experimentally, from pivot axis of model)
P_s	Settling chamber reference pressure
P_w	Working section reference pressure
q	Kinetic pressure
R_θ	Boundary layer Reynolds number, $u_e\,\theta/\nu$
s	Semi-span of wing
U	Reference freestream velocity
u	component of u_e in x direction
$\underline{u}$	Component of velocity within the boundary layer parallel to u_e
u_e	Local freestream velocity
w	Component of u_e in z direction
$\underline{w}$	Component of velocity within the boundary layer normal to u_e and parallel to ground plane
x	Co-ordinate parallel to freestream velocity vector
$\underline{x}$	Curvilinear co-ordinate parallel to local freestream
$\bar{x}$	Distance from pitch axis to intersection of line of force and wing chord line

y Co-ordinate normal to ground plane

z Co-ordinate normal to x in the plane of the ground

$\underline{z}$ Curvilinear co-ordinate normal to $\underline{x}$ in the plane of the ground

α Angle of incidence

Γ Circulation

$\Delta\alpha$ Induced incidence

ΔC_L Defined in Section 3 as $\Delta C_L = C_L - (C_L)_{\alpha=-4^\circ}$ for Model 3. Also defined in Section 4 as the difference between C_L and the inviscid value of C_L

ΔC_D Defined in Section 3 as $\Delta C_D = C_D - (C_D)_{\alpha=-4^\circ}$ for Model 3

δ Boundary layer thickness

δ^* The displacement thickness of the ground board boundary layer measured in the absence of the model beneath the model position (experimentally, beneath pivot axis of model)

$\underline{\delta}^*$ Displacement thickness of threedimensional boundary layer

δ_1 $$\delta_1 = \int_0^{\delta} \left(1 - \frac{\underline{u}}{u_e}\right) dy$$

δ_2 $$\delta_2 = -\int_o^{\delta} \frac{\underline{w}}{u_e} dy$$

θ, θ' See Fig. 34 for definitions

ν Kinematic viscosity of fluid

ρ Density of fluid

τ_o Wall shear stress

ϕ An unspecified aerodynamic function concerning the model

REFERENCES

No.	*Author(s)*	*Title, etc.*
1	A. de Sievers	Etude en soufflerie de l'effect de sol. ONERA Note Technique 87 (1965).
2	S. F. J. Butler, B. May and T. Pound ..	A moving-belt rig for ground simulation in low speed wing tunnels. A.R.C. R. & M. 3451 (1963).
3	J. Williams and S. F. J. Butler	Further developments in low-speed wind tunnel techniques for V/STOL and high-lift model testing. R.A.E. Technical Note Aero 2944. A.R.C. 25849 (1964).
4	H. Werlé	Simulation de l'effet de sol au tunnel hydrodynamique. ONERA TP 63. La Recherche Aeronautique **95**, p. 7–15 (1963).
5.	J. A. Bagley	The pressure distribution on twodimensional wings near the ground. A.R.C. R. & M. 3238 (1960).
6	D. L. I. Kirkpatrick	Experimental investigation of the ground effect on the subsonic longitudinal characteristics of a delta wing of aspect ratio 1·616. R.A.E. Technical Report 66179 (1966). A.R.C. 28407.
7	P. D. Smith	R.A.E. unpublished.
8	M. N. Wood	Private communication.
9	R. C. Hastings and R. G. Maulden	Private communication.
10	D. Küchemann, J. Weber and G. G. Brebner	Low speed tests on wing of 45° sweep—Part II. Balance and pressure measurements on wings of different aspect ratio. A.R.C. R. & M. 2882 (1951).
11	G. G. Brebner	Boundary layer measurements on wings of 45° sweep at low speed. R.A.E. Technical Note Aero 2298 (1954).
12	D. J. Kettle	The low speed effects of fuselage length and cross-section size on the aerodynamic characteristics of subsonic transport aircraft of large capacity. R.A.E. Technical Report to be published.
13	D. A. Lovell	A low speed wind-tunnel investigation of the tail-plane effectiveness of a model representing the Airbus type of aircraft. A.R.C. R. & M. No. 3642 (1969).
14	A. M. O. Smith and J. L. Hess	*Calculations of potential flow about arbitrary bodies. Progress in Aeronautical Sciences*, Vol. 8 (1966).
15	M. R. Head	Entrainment in the turbulent boundary layer. A.R.C. 20383, R. & M. 3152 (1958).

16 M. J. Lighthill . . . . . On displacement thickness.
Journal Fluid Mech. 4, 383–392 (1958).

17 L. F. East and R. P. Hoxey . . Low-speed threedimensional turbulent boundary layer data—Part 1.
A.R.C. R. & M. 3653 (1969).

APPENDIX I

Calibration Procedure
(*see* Section 3.1)

The presence of a ground board in the working section of a wind tunnel splits the section into two parts. Calibration is therefore required to obtain the true dynamic pressure in the section containing the model. Providing the ground board does not extend so far forward in the working section for its upstream influence to affect the working section reference tapping (P_w), the total flow through the working section can be deduced from the reference pressure difference ($P_s - P_w$) in the normal way. For any particular ground board configuration and tunnel reference pressure difference, the static pressure at the model position and at a selected position on the opposite side of the ground board are measured relative to P_w with the model removed from the tunnel. From the static pressures, changes in the dynamic pressures can be deduced since it is assumed that the total pressure distribution will not be changed by the presence of the model. For each model attitude, the change of dynamic pressure (δq_2) is measured on the empty side of the ground board and from this measurement the change of dynamic pressure at the model (δq_1) can be deduced by continuity. The relationship is,

$$\delta q_1 = -\frac{A_2}{A_1}\sqrt{\frac{q_1}{q_2}}\,\delta q_2 \tag{A.1}$$

where suffix 1 refers to the section of the tunnel enclosing the model and suffix 2 to the section on the opposite side of the ground board (*see* Fig. 2). A is the cross-sectional area and q_1 and q_2 are taken as the dynamic pressures in the absence of the model.

This calibration procedure has been checked on measurements made on the same model (Model 1), at the same attitude but with widely differing circulation about the ground board[8]. The changes of circulation were produced by a large full-span flap attached to the trailing edge of the ground board. In addition to showing that the measurements obtained with different amounts of circulation about the ground board yielded the same force coefficients when the above calibration procedure was used, it was also demonstrated, by direct measurement, that at the measuring station the pressure gradient normal to the ground board at the centre of the working section was negligible for the length of ground board used ($L = 2{\cdot}44$ m and 3·66 m). This observation justifies the use of the mean flow argument to derive equation (A.1) above.

Significant calibration errors should not occur unless the ground board is so short that the pressure field of the model influences the flow attaching to the leading edge of the ground board. If this happens to a sufficient extent, errors could arise from the resulting threedimensionality of the flow spreading back to the measuring station or the model. However, this configuration should not normally be used since errors will also arise because the ground board is too short to satisfactorily represent the ground.

This calibration procedure enables the appropriate dynamic pressure to be obtained for the section of the tunnel enclosing the model but it does not include any blockage or constraint correction.

The basis of this calibration procedure is the same as previously used in Refs. 6 and 9, and the validity of this procedure is supported by the detailed flow measurements of Hastings and Maulden[9].

APPENDIX II

The Dependence of C_L, C_D and $\bar{x}/c$ upon δ^*
(*see* Section 3.3)

A simple analysis is required to correlate the slopes of the lines through the experimental data shown in Figs. 6–17 and thereby obtain further insight into the fluid mechanics of the problem. As stated in Section 2, a thorough analysis of the threedimensional configuration would be very difficult and is not attempted here. Instead a simple analysis is proposed, based upon the concept that the influence of the boundary layer on low aspect ratio wings is primarily due to the large divergence of the boundary layer induced by the pressure field of the wing and its image, as discussed in section 5. This analysis is restricted therefore, to estimating the effect of the divergence of the boundary layer upon the flow about the wing.

Consider a wing of finite aspect ratio of mean chord c, semi-span s and circulation Γ positioned at a height h above a ground board in a uniform flow of velocity U. Assume that the boundary layer on the ground board in the absence of the wing is of constant displacement thickness δ^* along the length of the ground board.

The effect that the divergence of the local freestream will have on the boundary layer can be deduced from the definition of the displacement thickness of a threedimensional boundary layer which is given by the equation[16]:

$$\underline{\delta}^* = \delta_1 + \frac{1}{u_e}\frac{\partial}{\partial \underline{z}}\int_o^{\underline{x}} u_e \delta_2 \, d\underline{x}, \tag{B.1}$$

where $\underline{x}$ and $\underline{z}$ are respectively the streamline and orthogonal axes of a curvilinear co-ordinate system based on the freestream just outside the boundary layer. The integral is taken from the start of the boundary layer flow and δ_1 and δ_2 are the boundary layer integrals defined in the list of symbols. Since this analysis is restricted to configurations in which the effect of the divergence of the freestream dominates the development of the boundary layer, the variations of δ_1 and u_e with $\underline{x}$ and $\underline{z}$ can be ignored.
Hence differentiating equation (B.1) with respect to $\underline{x}$ gives,

$$\frac{\partial \underline{\delta}^*}{\partial \underline{x}} = \frac{\partial \delta_2}{\partial \underline{z}}. \tag{B.2}$$

For this type of steadily diverging flow it has been found[17] that δ_2 is given by,

$$\frac{\delta_2}{\delta_1} = -2\tan^{-1}\left(\frac{w}{U+u}\right), \tag{B.3}$$

where $(U+u)$ and w are respectively the longitudinal (x) and transverse (z) components of the local freestream. Equation (B.3) can be approximated to,

$$\delta_2 \simeq -2w\,\delta^*/U, \tag{B.4}$$

because δ_1 is assumed to be invariant with $\underline{x}$ and $\underline{z}$ and so can be put equal to δ^*, $u \ll U$ and w/U is assumed small. Substituting equation (B.4) into equation (B.2) gives,

$$\frac{\partial \underline{\delta}^*}{\partial \underline{x}} = -\frac{2\delta^*}{U}\frac{\partial w}{\partial \underline{z}}. \tag{B.5}$$

Since the angle of yaw of the local freestream outside the ground boundary layer will, in most practical cases, be small (less than 0·1 radian say), equation (B.5) can be written directly in rectangular co-ordinates without significant loss of accuracy. Thus

$$\frac{\partial \underline{\delta}^*}{\partial x} = -\frac{2\delta^*}{U}\frac{\partial w}{\partial z}. \tag{B.6}$$

gives the slope of the displacement surface in the undisturbed flow direction as a function of the local transverse flow velocity.

The transverse component of the freestream velocity induced by the wing and its image in the ground board plane just outside the ground board boundary layer, can be expressed in the general form,

$$w = \frac{\Gamma}{h}\cdot f(s/h, x/c, z/s) \tag{B.7}$$

which can be substituted into equation (B.6) to give,

$$\frac{\partial \underline{\delta}^*}{\partial x} = -\frac{2\delta^*}{U}\cdot\frac{\Gamma}{hs}\cdot\frac{\partial f}{\partial(z/s)}. \tag{B.8}$$

The variation of the height of the displacement surface of the boundary layer will induce upwash velocities at the wing position. For this type of steadily-diverging threedimensional boundary layer the displacement surface will have a fairly uniform slope over the planform area of the wing. If the wing were positioned very close to the ground the induced incidence would be approximately $(\partial\underline{\delta}^*/\partial x)$, but as the height is increased the induced incidence will decrease. The simplifying assumption is made that over the limited range of h/s covered by the experimental data of Section 3 the upwash at the wing is proportional to s/h, though this will clearly be in error for very large values of s/h. Hence the induced incidence at the wing $(\Delta\alpha)$ is given by,

$$\Delta\alpha(x/c, z/s) \propto \frac{s}{h}\frac{\partial \underline{\delta}^*}{\partial x}. \tag{B.9}$$

Combining equation (B.8) with equation (B.9) gives the induced incidence at points on the wing as,

$$\underline{z}\Delta\alpha(x/c, z/s) \propto \frac{\delta^*\Gamma}{Uh^2}\frac{\partial f}{\partial(z/s)} \propto \frac{\delta^* c\, C_L}{h^2}\frac{\partial f}{\partial(z/s)}. \tag{B.10}$$

It is assumed that the lift and drag coefficients are primarily dependent upon a mean induced incidence and that the induced camber effects are small. The mean induced incidence is given by,

$$\Delta\alpha \propto \frac{\delta^* c\, C_L}{h^2}\cdot F(s/h),$$

where $F(s/h)$ is an integral of $\partial f/\partial(z/s)$ over the wing planform. In general F will be a function of s/h but as the variation of s/h for the three models tested in Section 3 is small $(3{\cdot}5 < s/h < 5)$ F can be treated as a constant (K_1) for the present purposes*. This induced incidence will result in a change of lift coefficient (δC_L) given by,

---

* Support for this assumption can be obtained by analysing a simple horseshoe vortex positioned near the ground. The mean induced incidence across the span is obtained by integrating equation (B.10) to give,

$$\Delta\alpha(x/c) \propto \frac{\delta^* c\, C_L}{h^2}(f)_{z/s\,=\,1},$$

and it is readily shown that if $2s/h > 1$ then for a simple horseshoe vortex.

$$(f)_{z/s\,=\,1} \simeq \frac{1}{2\pi}\left(1+\frac{x}{\sqrt{x^2+h^2}}\right).$$

Thus $(f)_{z/s\,=\,1}$ and F are not strongly dependent upon s/h.

$$\delta C_L = \left(\frac{\partial C_L}{\partial \alpha} + C_D\right)\Delta\alpha \simeq \frac{\partial C_L}{\partial \alpha}\Delta\alpha \tag{B.11}$$

since in general $\frac{\partial C_L}{\partial \alpha} \gg C_D$, and in a change of drag coefficient (δC_D) given by

$$\delta C_D = \left(\frac{\partial C_D}{\partial \alpha} - C_L\right)\Delta\alpha\,. \tag{B.12}$$

Substituting for $\Delta\alpha$, equations (B.11) and (B.12) can be written in the more convenient forms.

$$\frac{\partial C_L}{\partial(\delta^*/h)} = K_1(C_L\, c/h)\frac{\partial C_L}{\partial \alpha}. \tag{B.13}$$

and

$$\frac{\partial C_D}{\partial(\delta^*/h)} = K_1(C_L\, c/h)\left(\frac{\partial C_D}{\partial \alpha} - C_L\right). \tag{B.14}$$

The data obtained in Section 3 show that at the higher incidences the variation of the position of the centre of pressure ($\bar{x}/c$) with incidence is small and calculations using the induced incidence, $\Delta\alpha$, due to the boundary layer on the ground board, yield results very much smaller than the measured values of $(\partial(\bar{x}/c)/\partial(\delta^*/h))$. It is therefore assumed that these variations of $\bar{x}/c$ are primarily caused by the induced camber rather than by the mean induced incidence. If it is assumed that the increment of lift at a point on the wing is proportional to the induced incidence at the point, then, as the pitching moment about the new centre of pressure $(\bar{x}/c + \delta(\bar{x}/c))$ will be zero,

$$C_L\,\delta(\bar{x}/c) \simeq \frac{\delta^*\, c\, C_L}{h^2} \cdot G\,(s/h)\,, \tag{B.15}$$

where $G(s/h)$ is an integral of $\partial f/\partial(z/s)$ over the wing planform and can be assumed constant (K_2) by the same reasoning as given above for $F(s/h)$. Equation (B.15) can then be written in the more convenient form,

$$\frac{\partial(\bar{x}/c)}{\partial(\delta^*/h)} = K_2\, c/h\,. \tag{B.16}$$

APPENDIX III

The Twodimensional Development of the True Ground Boundary Layer
(*see* Section 4)

The procedure used for calculating the development of the boundary layer induced on a fixed surface by a twodimensional aerofoil passing by is outlined in this Appendix. The method used is an extension of the entrainment method[15], which was used to calculate the ground board boundary layer in Section 4.

The boundary layer which grows on a fixed surface under the influence of a moving aerofoil is time dependent. However, the time dependency can be removed by superimposing an equal and opposite velocity to that of the aerofoil. This reduces the aerofoil to rest in a uniform flow which is bounded on one side by a surface moving with the undisturbed flow velocity as shown in Fig. 30. Also shown in Fig. 30 are sketches of the boundary layer profiles at various stages of its development and in Fig. 34 various parameters are defined which are required in the analysis. The 'reverse' profile indicated in Fig. 34 is the real profile that occurs on the fixed ground. The reverse profile starts upstream of the aerofoil, Fig. 30, and grows as the aerofoil is approached under the influence of the negative pressure gradient ($\partial u_e/\partial x < 0$) which is favourable to the reverse profile. Downstream the pressure gradient becomes positive ($\partial u_e/\partial x > 0$ and hence adverse to the reverse profile) which leads to the reverse profile acquiring the shape of a separation profile. This represents the downstream limit of the calculation method but does not represent a catastrophic breakdown of the flow as would occur with a true separation but merely the moment when the flow close to the surface is stationary as it changes from flowing in the same direction as the aerofoil, to flowing in the opposite direction. Under the influence of the remaining positive pressure gradient a 'wall jet' type of profile will develop which will finally decay away far downstream because of the action of viscosity. It is interesting to note that in the real flow, in which the aerofoil moves and the ground is fixed, the residual flow well behind the aerofoil is similar to a wall jet moving in the opposite direction to the aerofoil.

The calculation method makes use of the momentum integral equation, an auxiliary 'entrainment' equation and an empirical skin friction relationship. In order to solve the present problem the standard R.A.E. computer programme for calculating boundary layer development by the entrainment method was modified to incorporate these equations in the following recast forms.

The momentum integral equation, which is exact within the normal boundary layer assumptions, can be applied unchanged to this flow. It can be written[15],

$$\frac{d\theta}{dx} = \frac{C_f}{2} - (H+2)\frac{\theta}{u_e}\frac{du_e}{dx} \tag{C.1}$$

where θ, H and u_e are defined in Fig. 34 and $C_f = \tau_o/\frac{1}{2}\rho u_e^2$.

The entrainment equation is based on the assumption that the rate at which fluid is entrained into the boundary layer is a universal function of the boundary layer profile. The rate of fluid entrainment is simply $d/dx\,(u_e H_1\,\theta)$ as normal, but in order that the standard empirical form of the functional dependence on the boundary layer profile can be used, this function must be written in terms of the 'reverse' profile. The modified entrainment equation then becomes,

$$\frac{d}{dx}(u_e H_1\,\theta) = (U-u_e)\,F(H_1'), \tag{C.2}$$

where H_1 and H_1' are the entrainment parameters defined in Fig. 34. Substituting for $d\theta/dx$ from equation (C.1) into equation (C.2) enables the entrainment equation to be written,

$$\frac{dH_1}{dx} = \frac{1}{\theta}\left\{\left(\frac{U-u_e}{u_e}\right)F - H_1\,C_f/2 + H_1(H+1)\frac{\theta}{u_e}\frac{du_e}{dx}\right\}. \tag{C.3}$$

The normal skin friction relationship used in the standard programme can be written in the form,

$$\tau_o/\rho\, u_e^2 = f(H, R_\theta)\,. \tag{C.4}$$

This relationship must be rewritten in terms of the reverse profile and it then becomes,

$$\tau_o/\rho(U-u_e)^2 = -f\left(H', \left|\frac{(U-u_e)\,\theta'}{\nu}\right|\right) \tag{C.5}$$

Using the relationship,

$$\theta' = -\frac{u_e\,(UH-u_e)\,\theta}{(U-u_e)^2}, \tag{C.6}$$

which can be deduced directly from the definitions given in Fig. 34 together with the definition of R_θ as $u_e\,\theta/\nu$, equation (C.5) can be rewritten as,

$$C_f/2 = \tau_o/\rho\, u_e^2 = \left(\frac{U-u_e}{u_e}\right)^2 f\left(H', \left|\left(\frac{UH-u_e}{U-u_e}\right)R_\theta\right|\right). \tag{C.7}$$

The standard R.A.E. programme was modified to incorporate equations (C.3) and (C.7), and was used to calculate the development of the boundary layer from a very small initial value till separation was predicted. This point, at which the skin friction changes direction was about a chord downstream of the trailing edge of the aerofoil. The curve of displacement thickness was then extrapolated downstream with a smooth curve so that the displacement thickness reduced to zero far downstream.

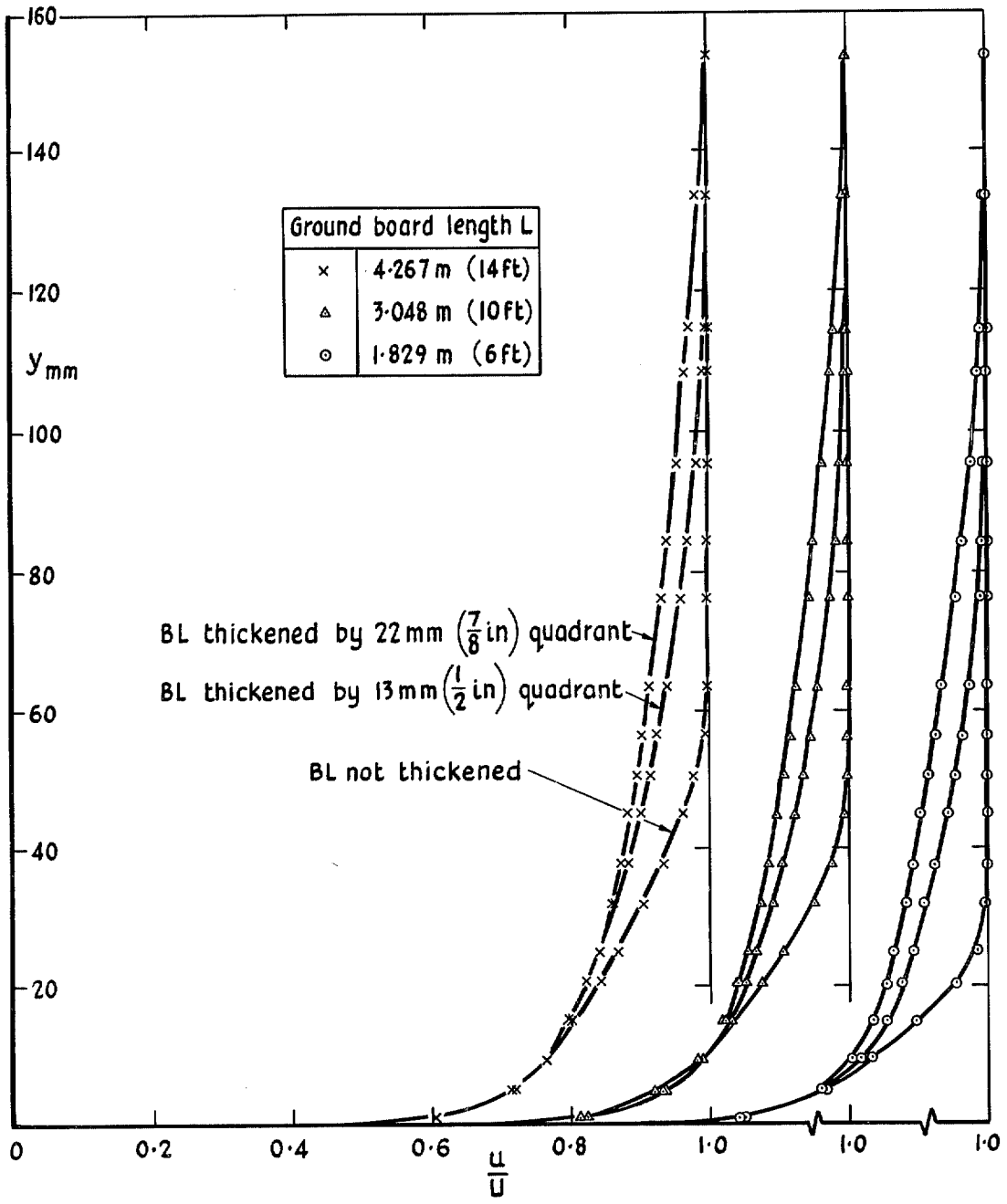

FIG. 1. Twodimensional boundary layer profiles on a ground board beneath the pivot axis of the model.

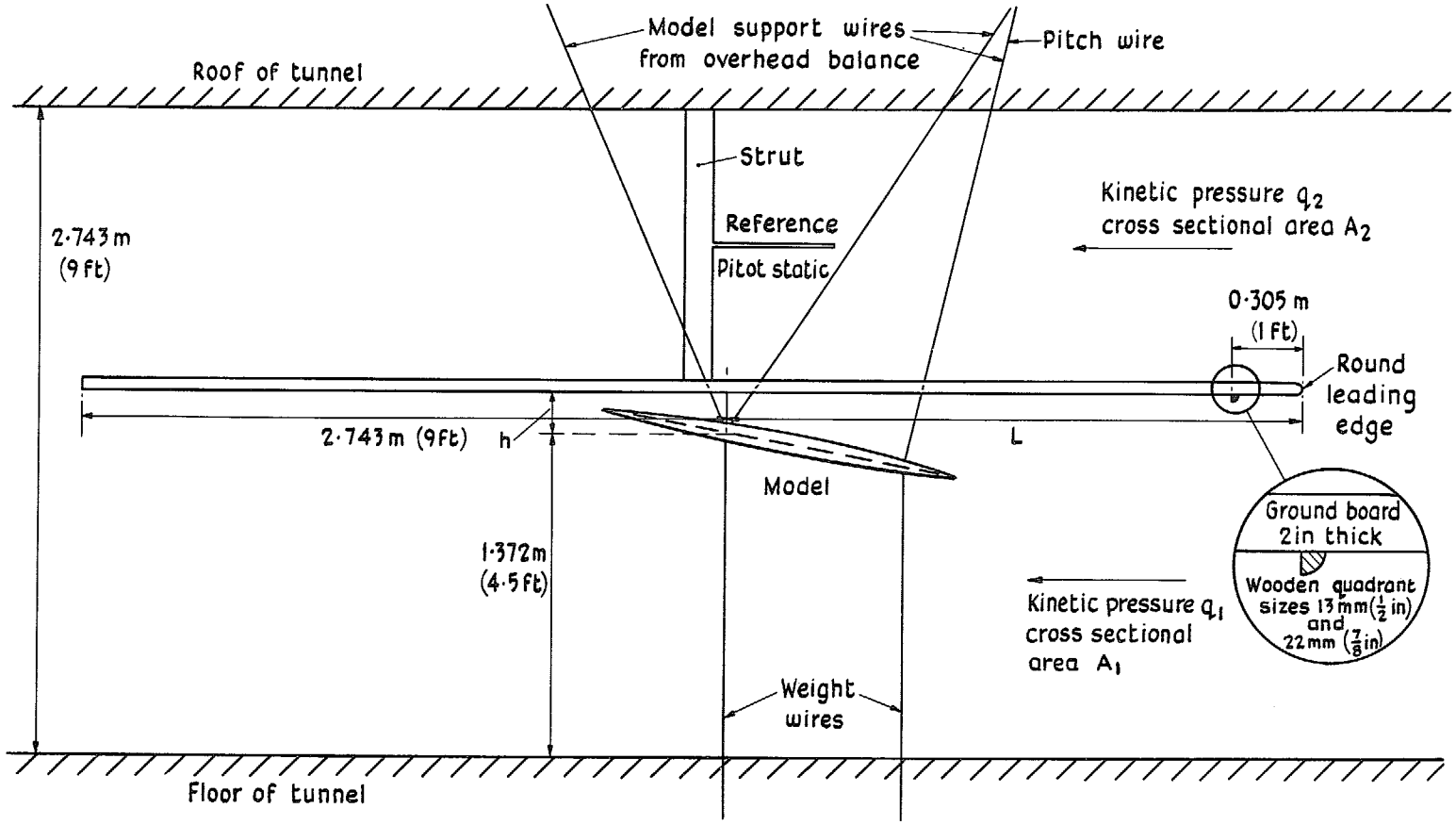

FIG. 2. General arrangement of model and ground board in 13ft × 9ft wind tunnel.

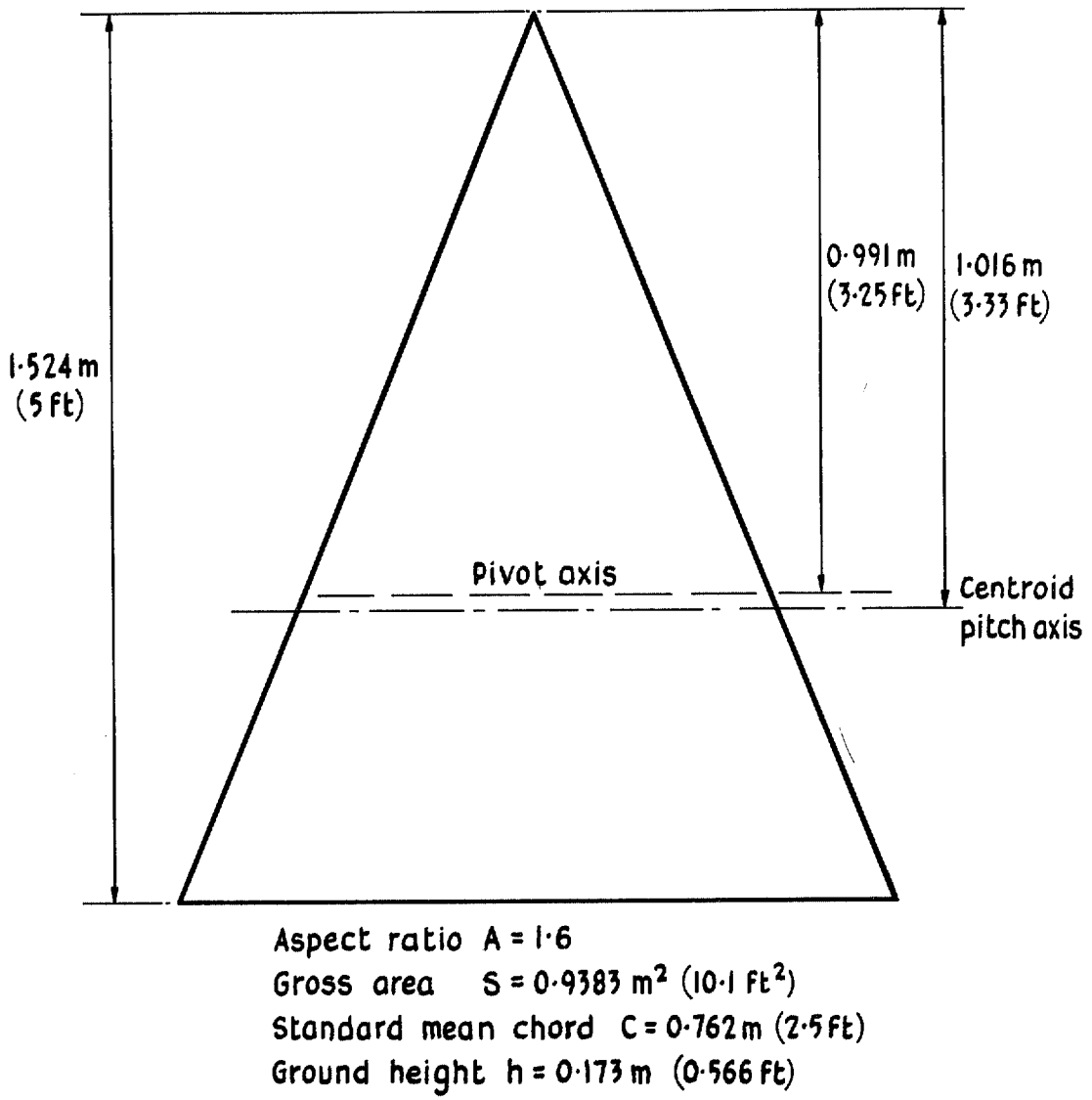

FIG. 3. Model 1. Planform and leading dimensions.

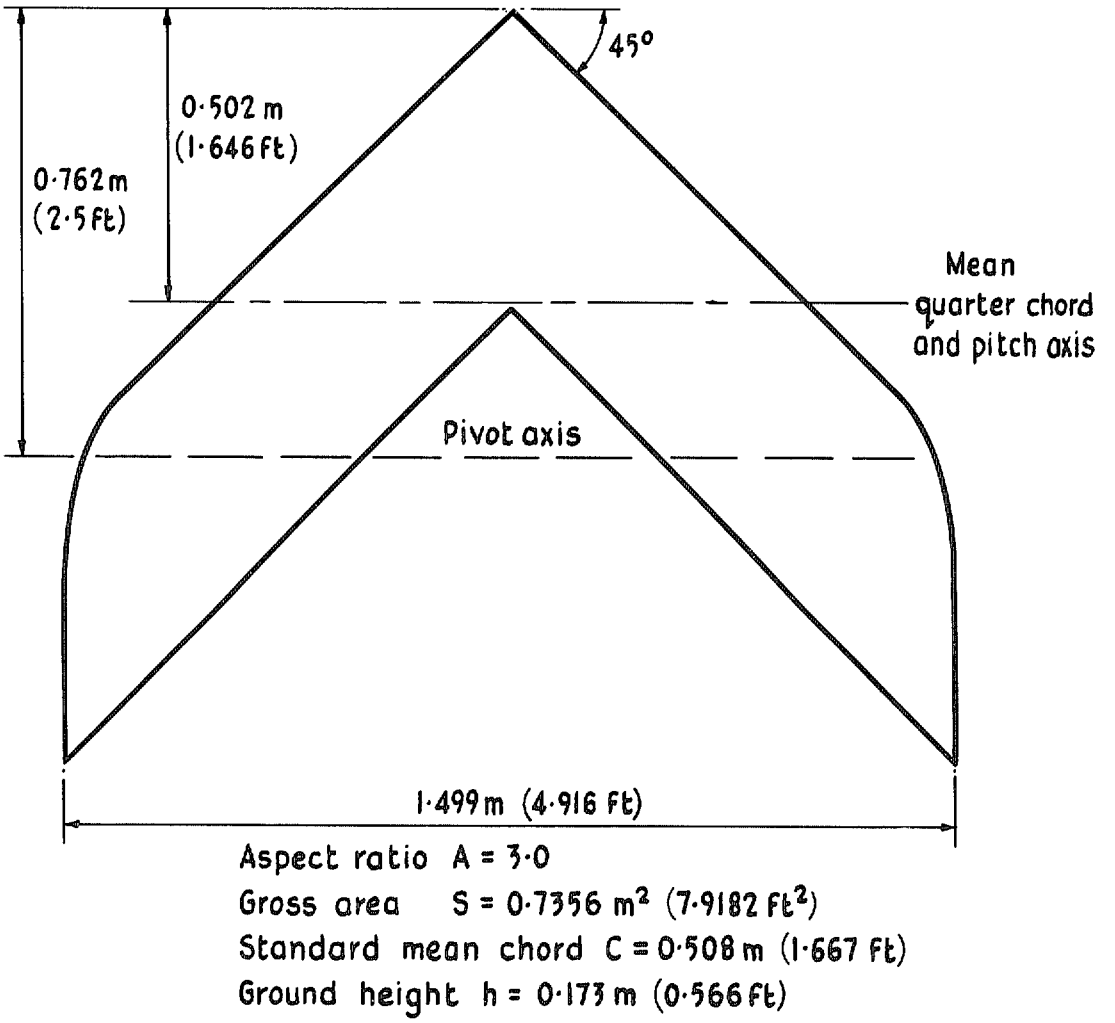

FIG. 4. Model 2. Planform and leading dimensions.

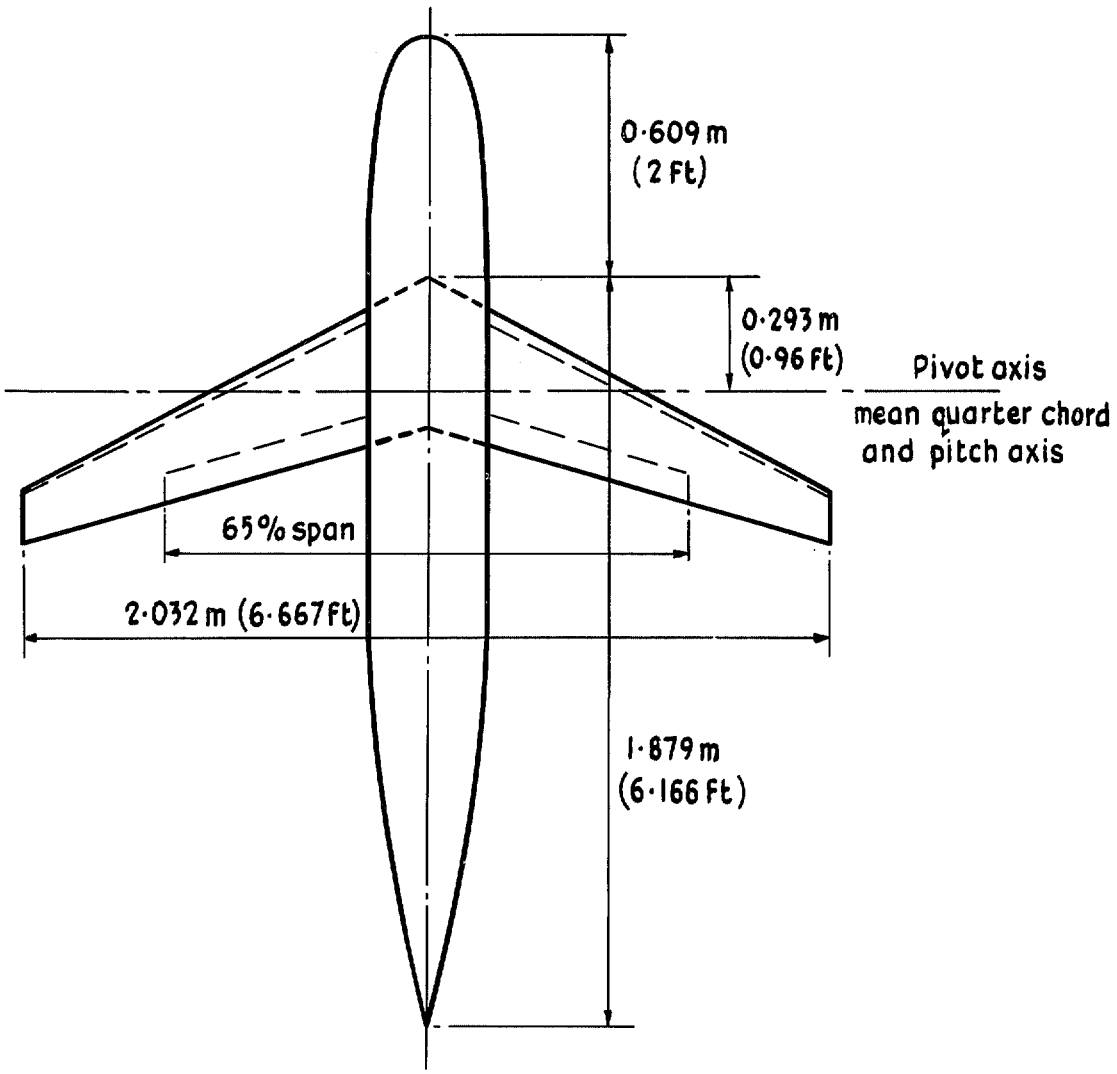

Aspect ratio A = 8
Gross area S = 0·5162 m² (5·556 Ft²)
Standard mean chord C = 0·254 m (0·833 Ft)
Ground height h = 0·202 m (0·662 Ft)

FIG. 5. Model 3. Planform and leading dimensions.

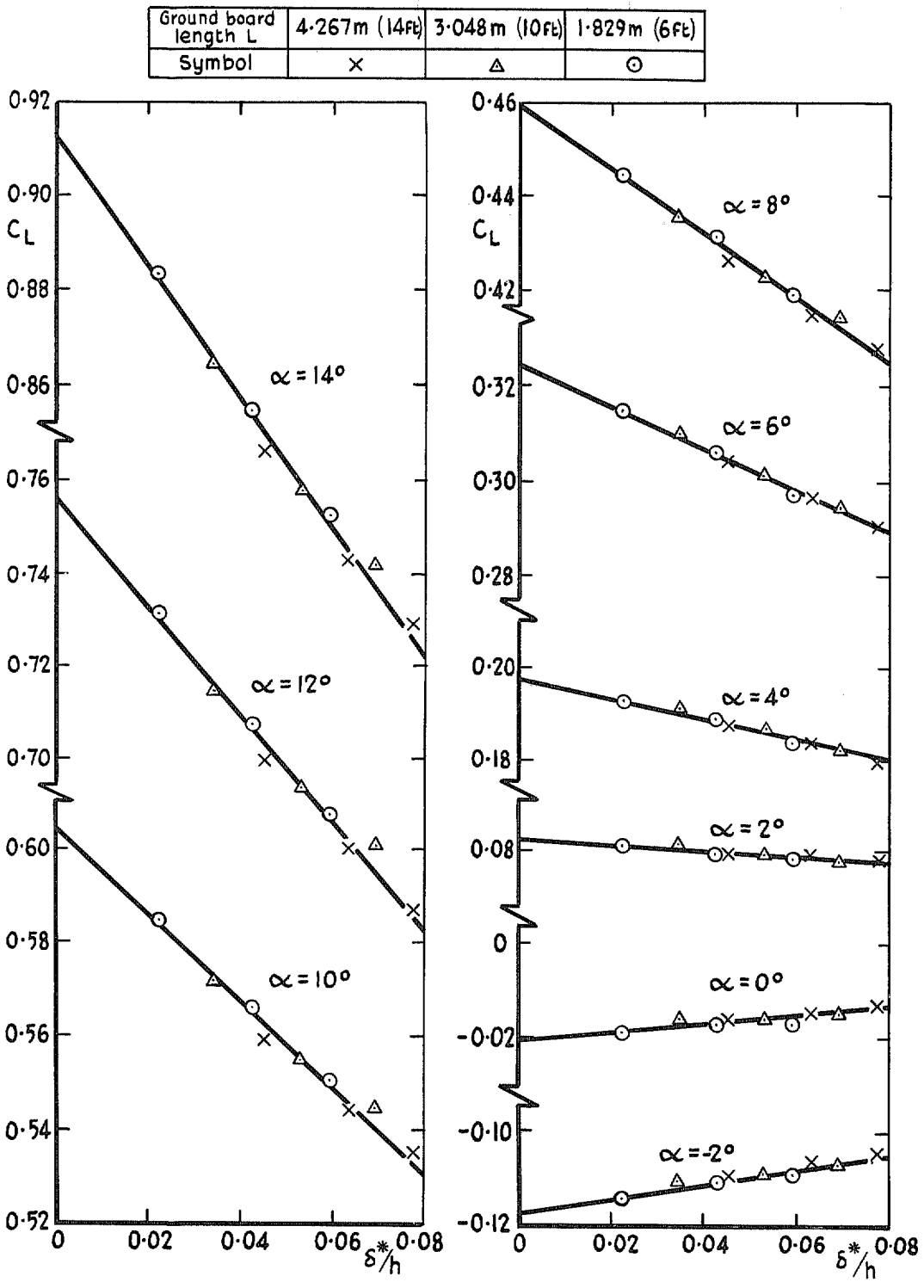

FIG. 6. Model 1. Dependence of C_L upon δ^*/h.

Ground board length L	4·267m (14Ft)	3·048m (10Ft)	1·829m (6Ft)
Symbol	×	△	⊙

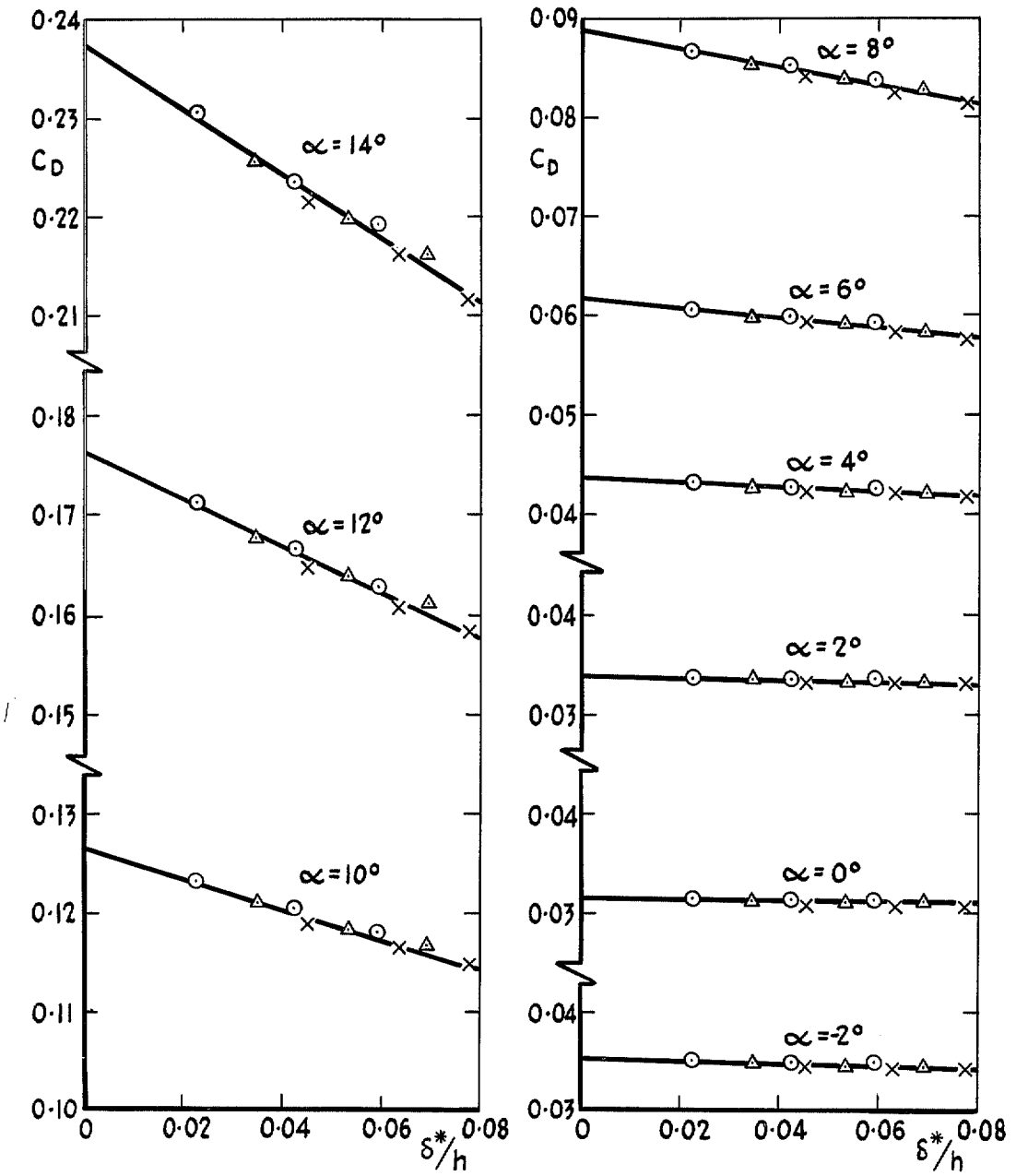

FIG. 7. Model 1. Dependence of C_D upon δ^*/h.

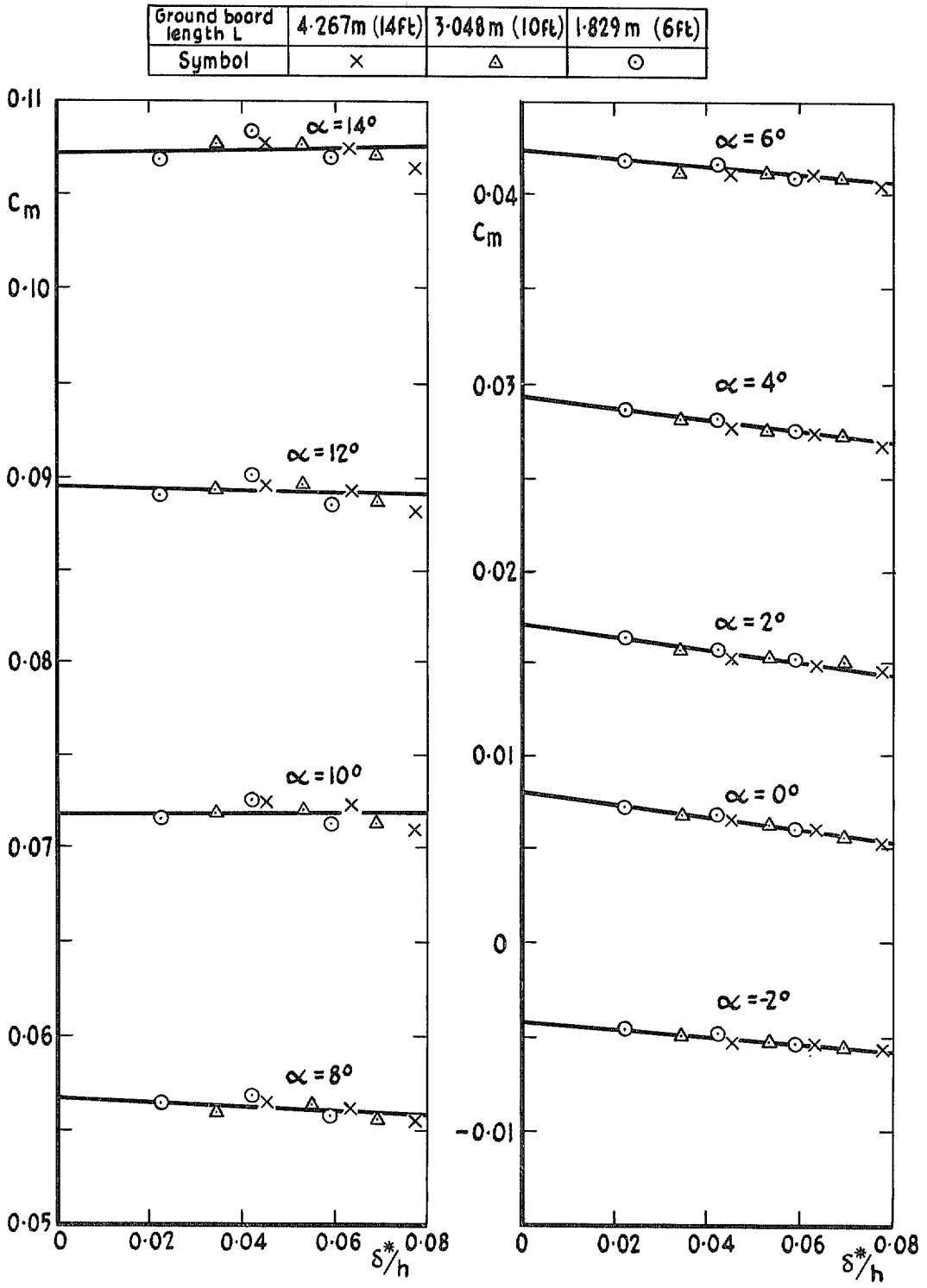

FIG. 8. Model 1. Dependence of C_m upon δ^*/h.

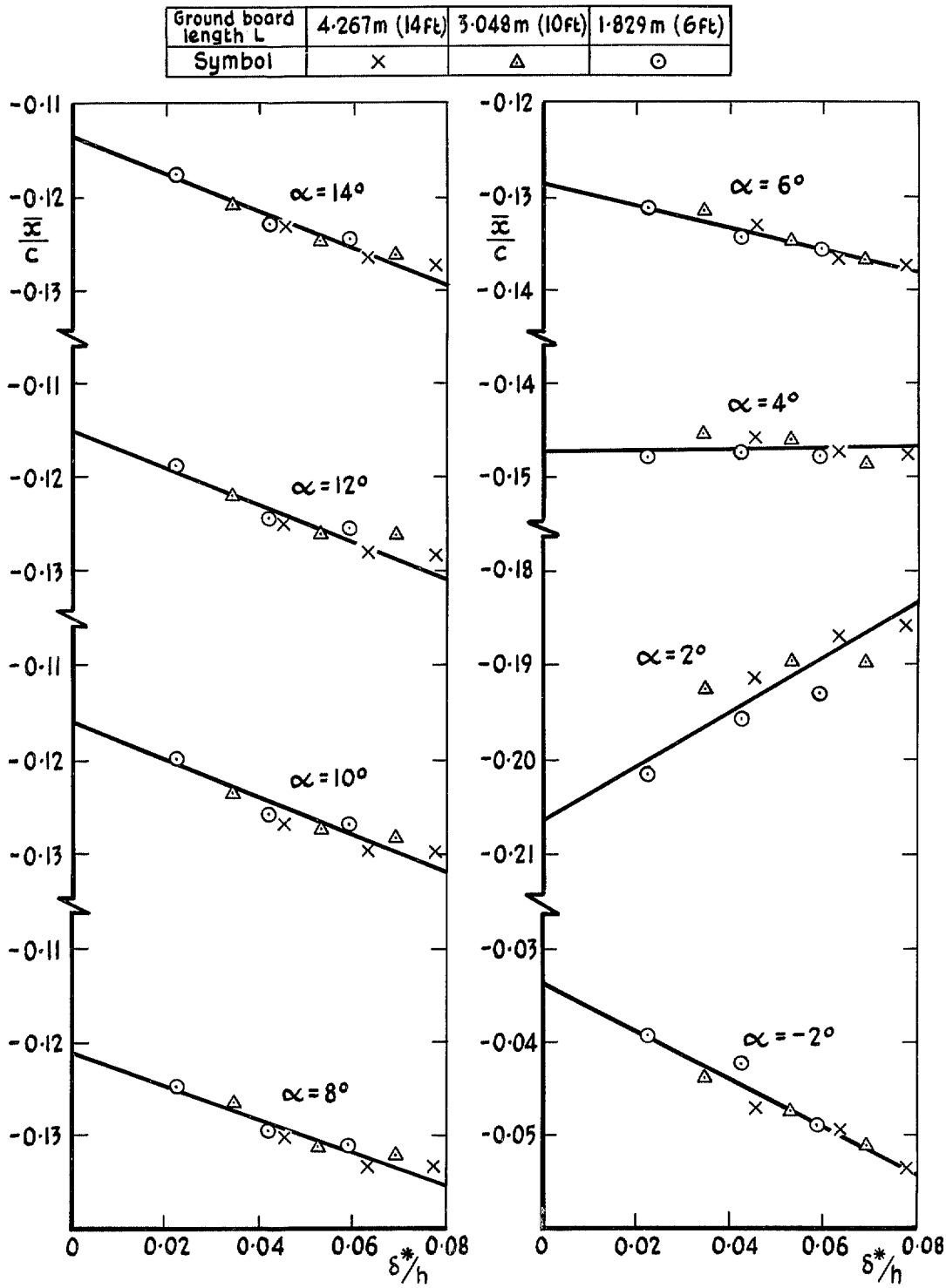

FIG. 9. Model 1. Dependence of $\frac{\bar{x}}{c}$ upon δ^*/h.

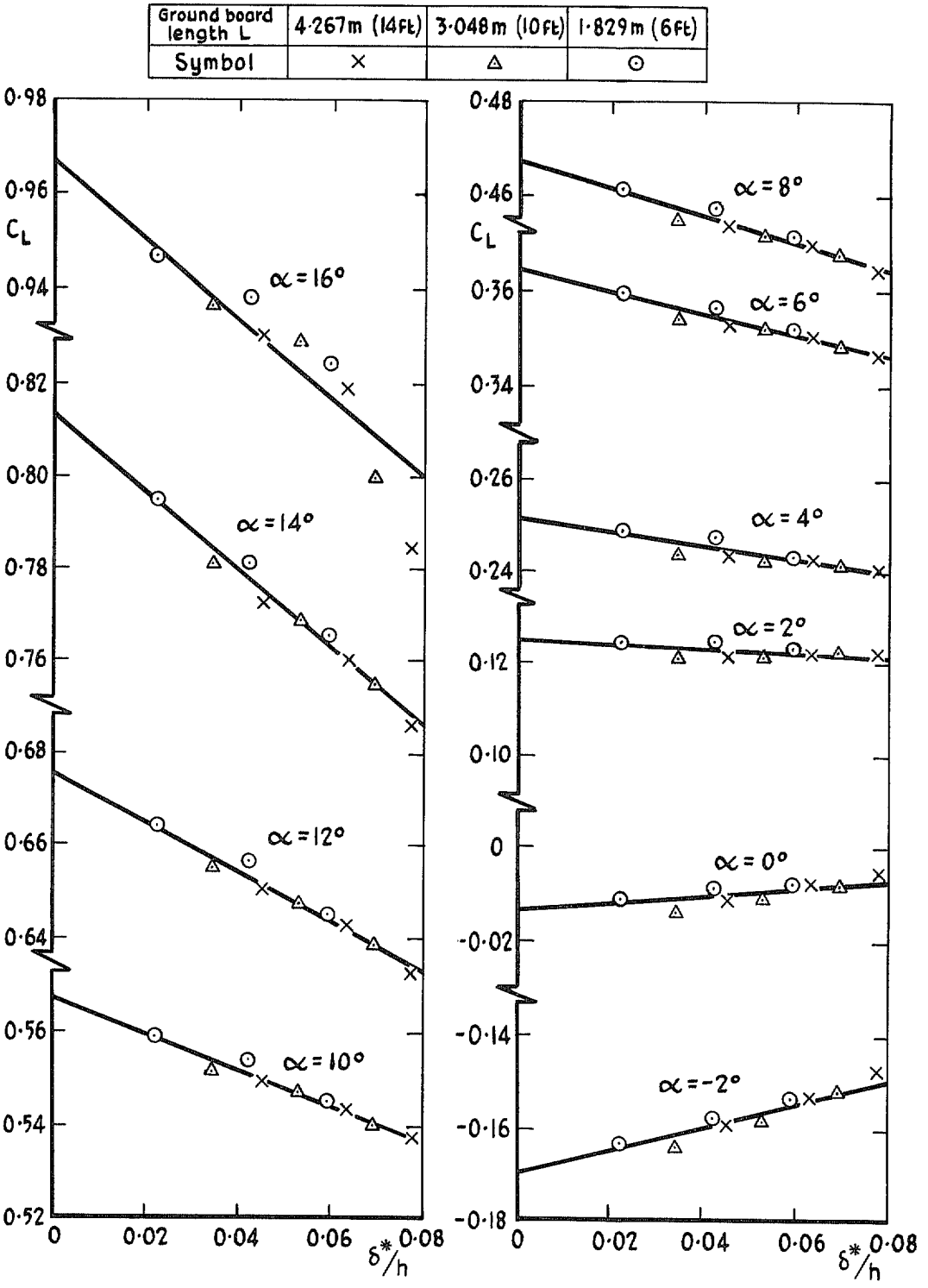

FIG. 10. Model 2. Dependence of C_L upon δ^*/h.

Ground board length L	4·267m (14Ft)	3·048m (10Ft)	1·829m (6Ft)
Symbol	×	△	⊙

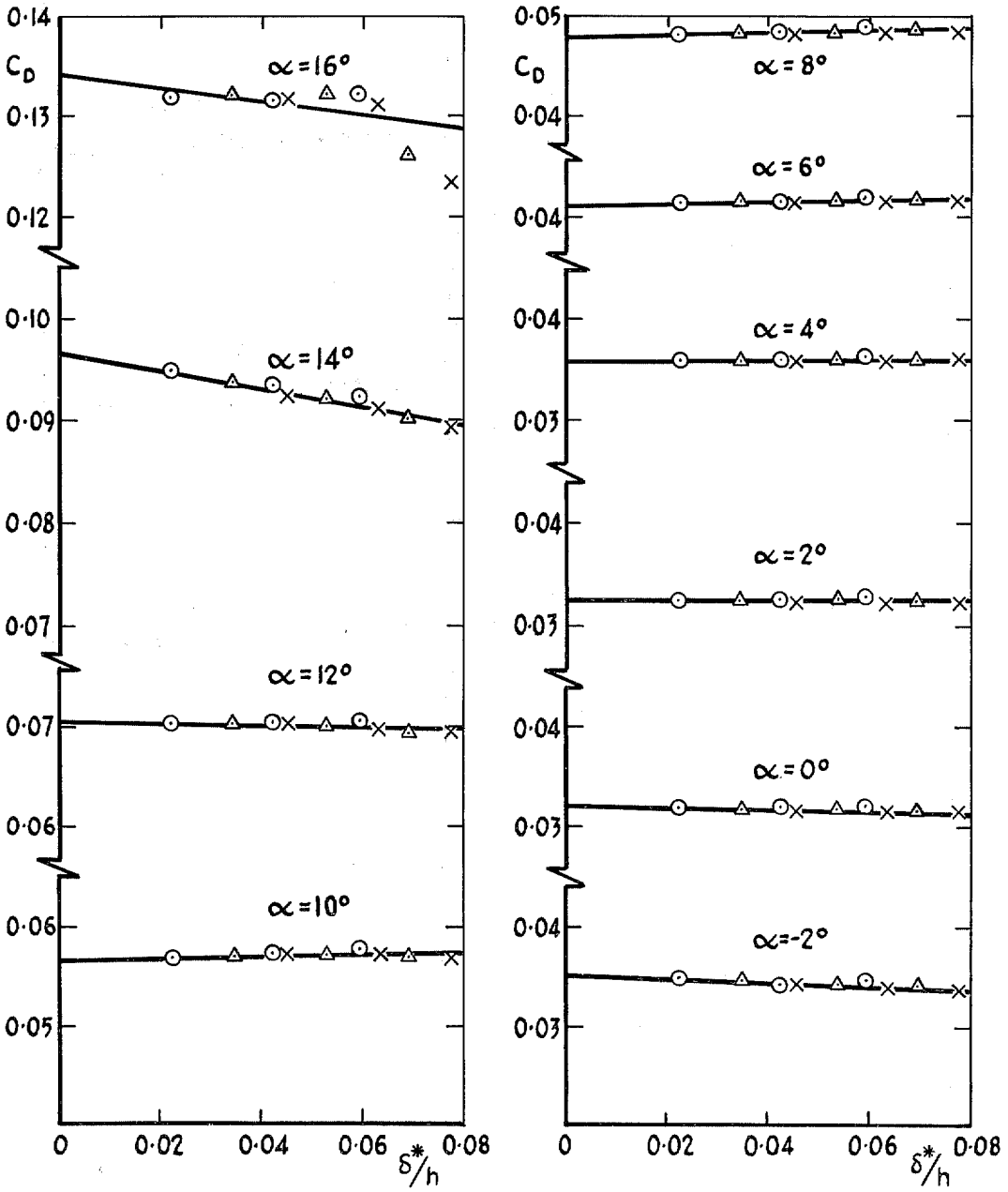

FIG. 11. Model 2. Dependence of C_D upon δ^*/h.

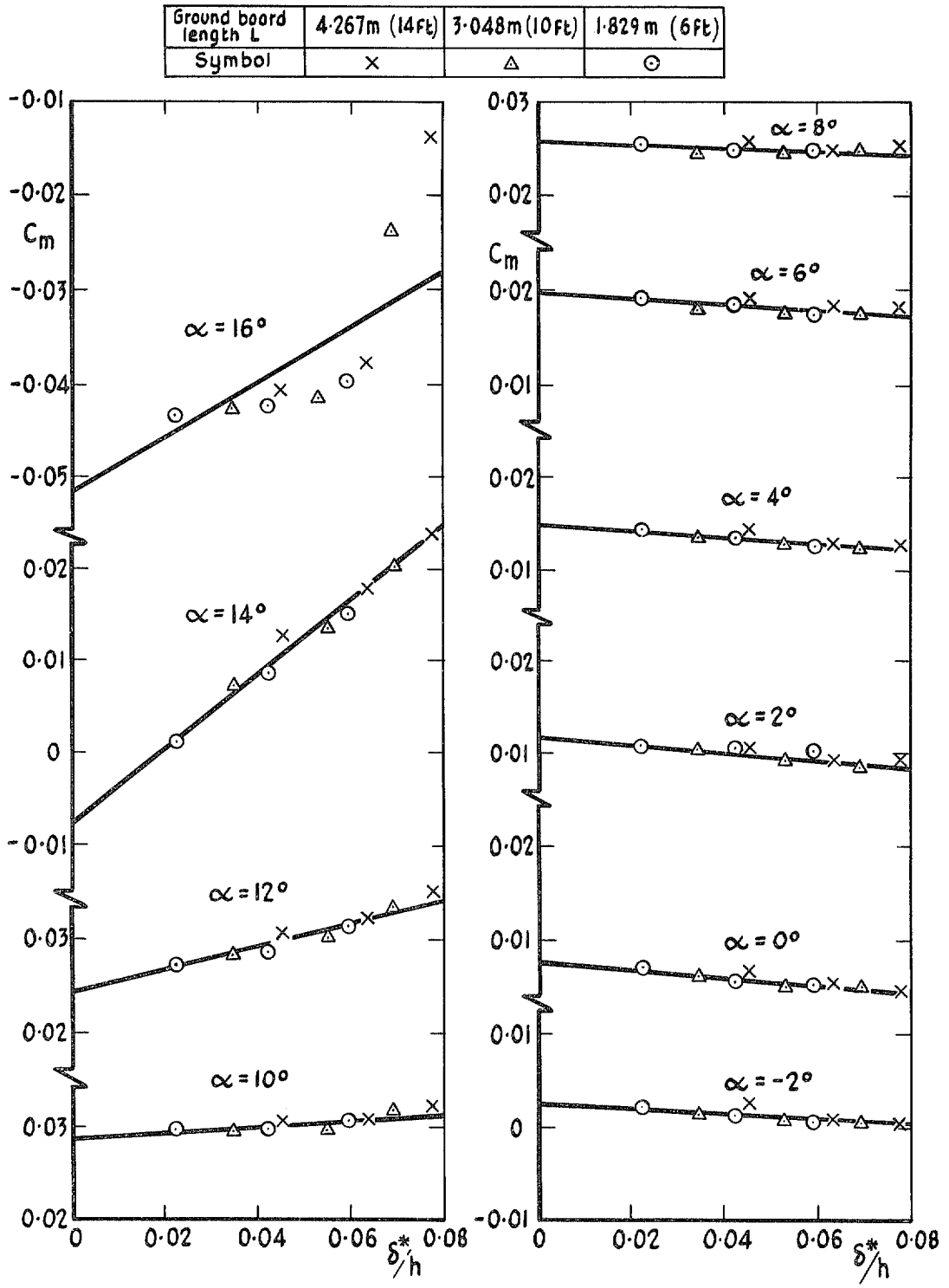

FIG. 12. Model 2. Dependence of C_m upon δ^*/h.

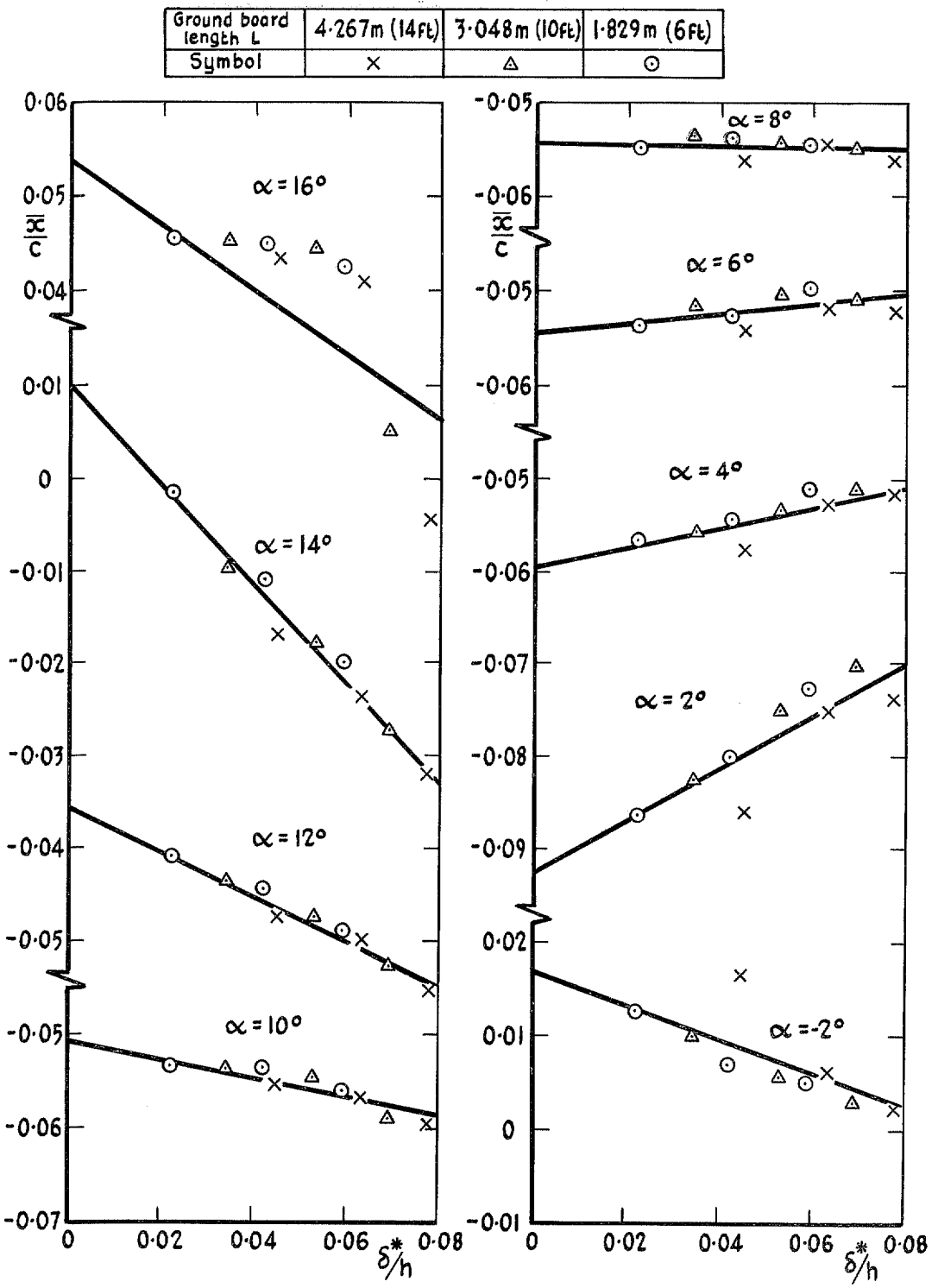

FIG. 13. Model 2. Dependence of $\frac{\bar{x}}{c}$ upon δ^*/h.

Ground board length L	4·267m (14Ft)	3·048m (10Ft)	1·829m (6Ft)
Symbol	×	△	⊙

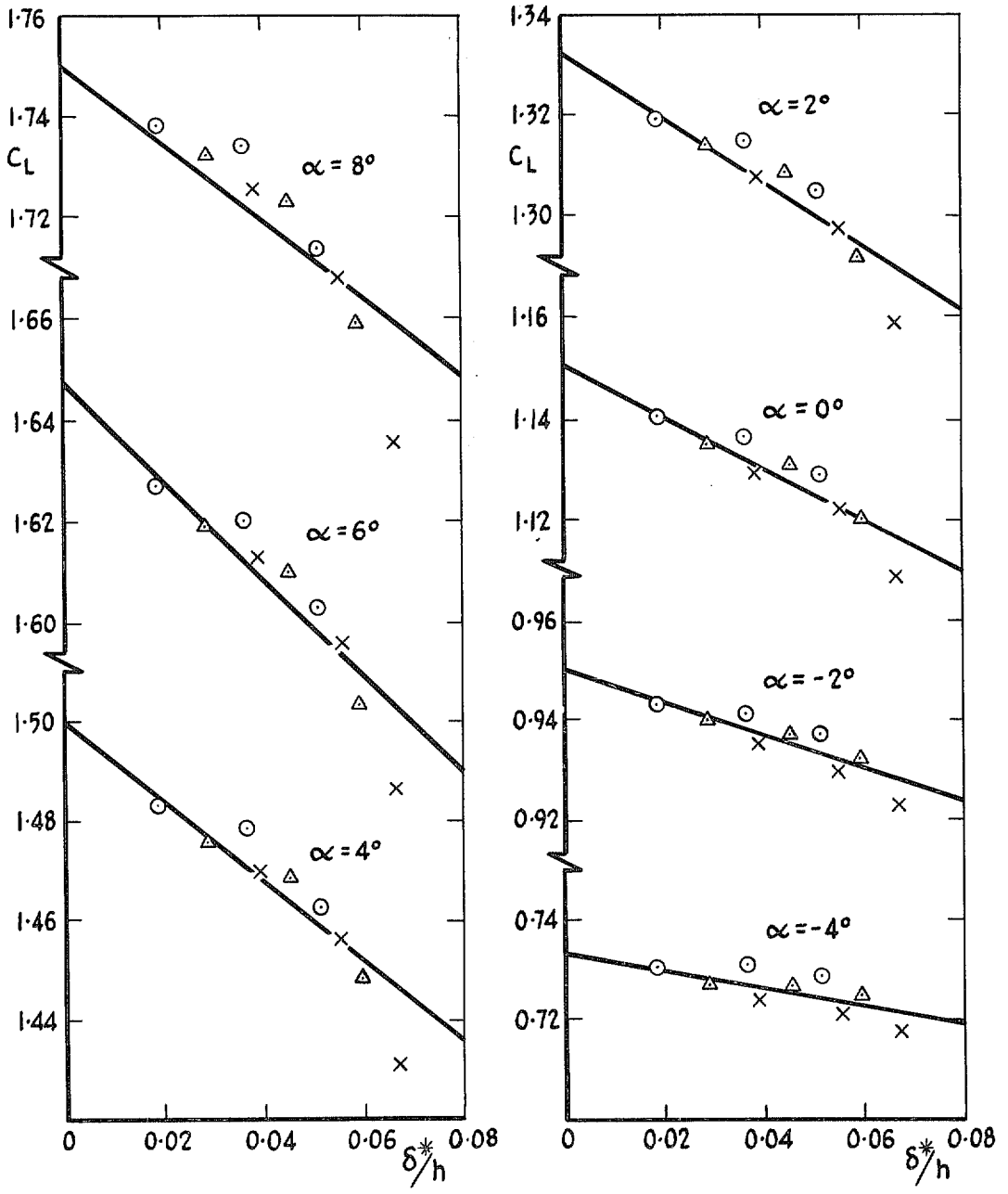

FIG. 14. Model 3. Dependence of C_L upon δ^*/h.

Ground board length L	4·267m (14Ft)	3·048m (10Ft)	1·829m (6Ft)
Symbol	×	△	⊙

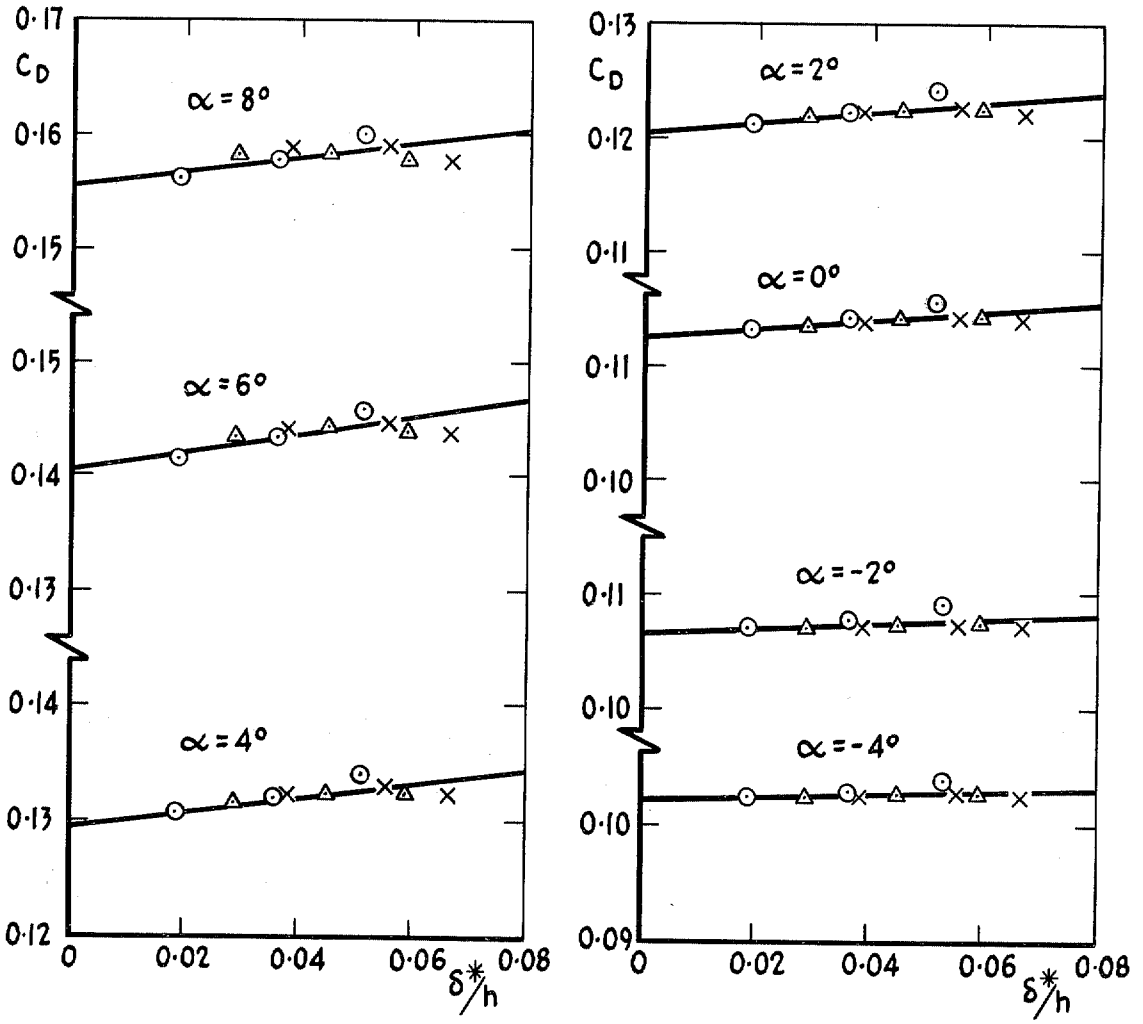

FIG. 15. Model 3. Dependence of C_D upon δ^*/h.

Ground board length L	4·267 m (14 ft)	3·048 m (10 ft)	1·829 m (6 ft)
Symbol	×	△	⊙

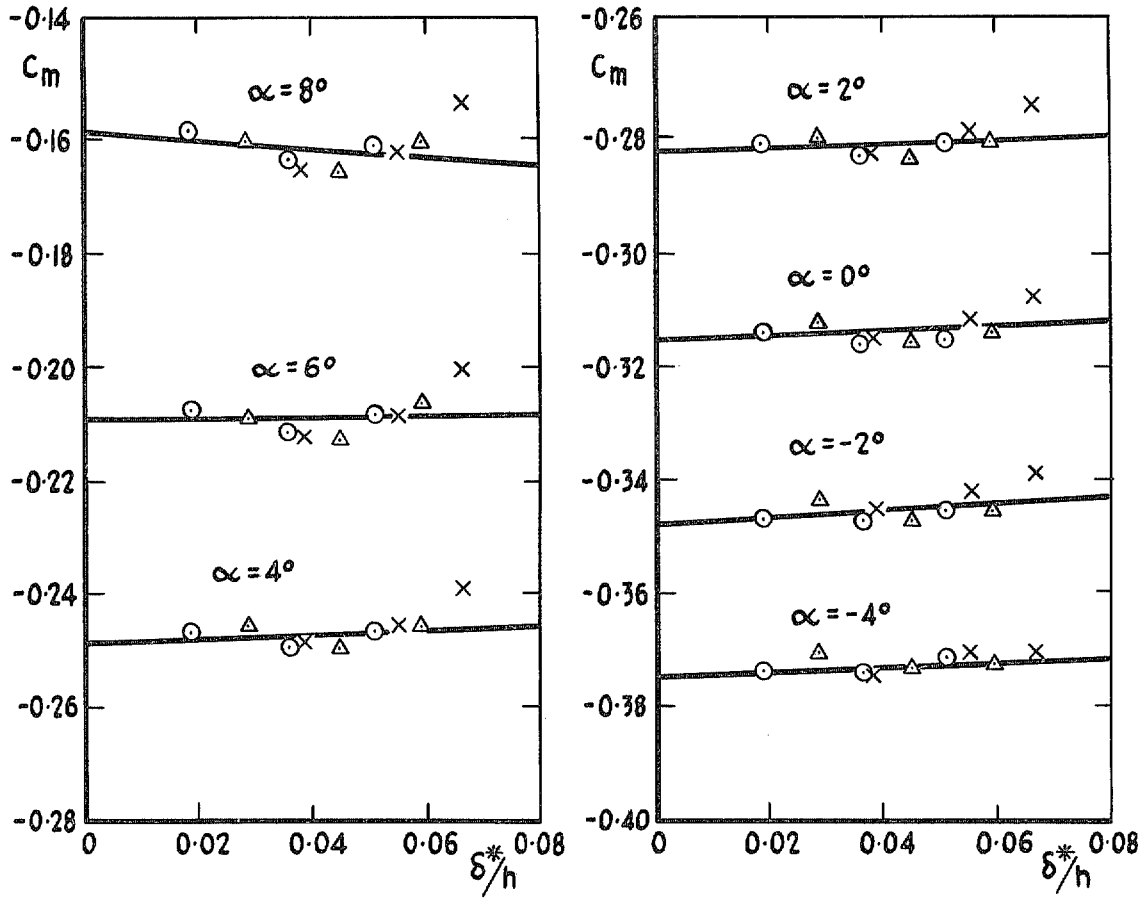

FIG. 16. Model 3. Dependence of C_m upon δ^*/h.

Ground board length L	4·267m (14Ft)	3·048m (10Ft)	1·829m (6Ft)
Symbol	×	△	⊙

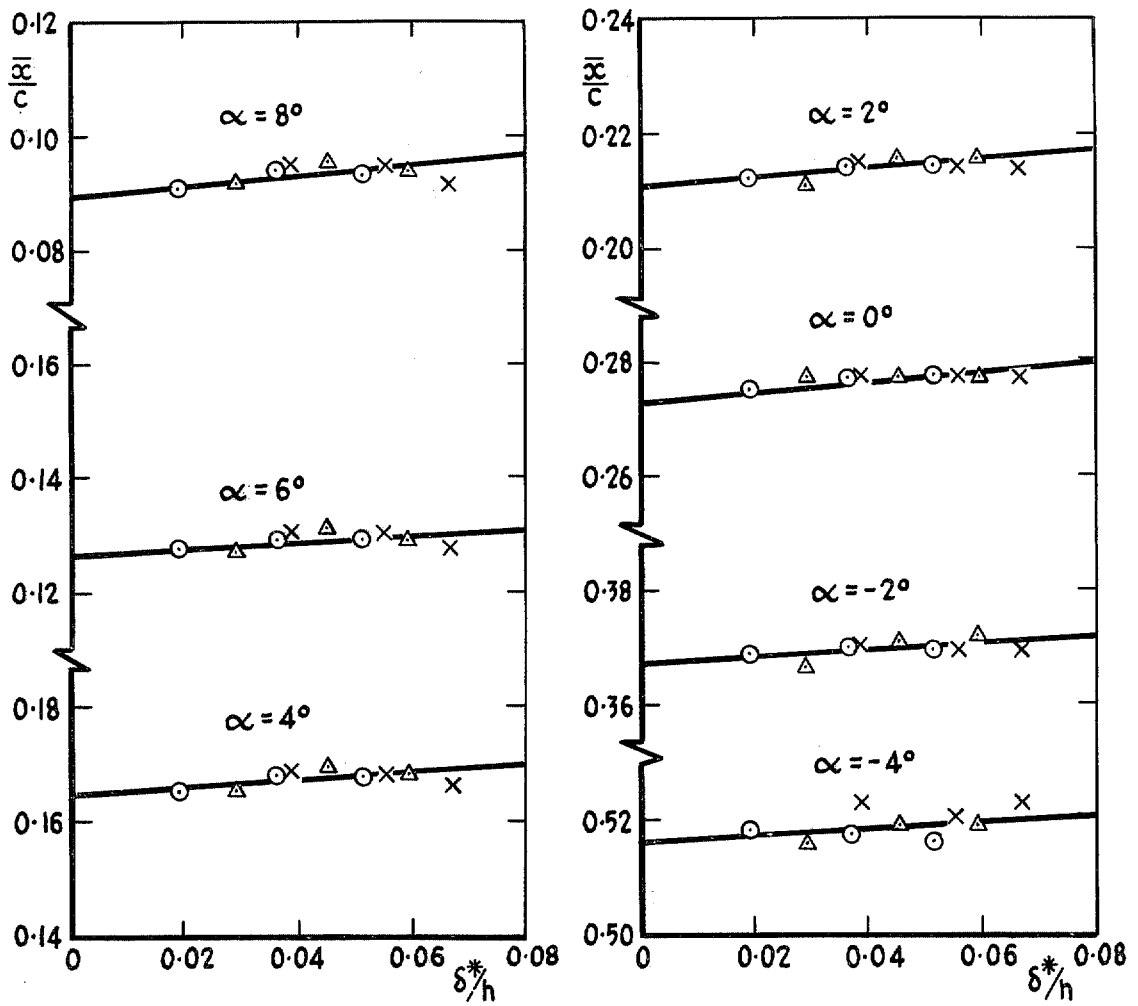

FIG. 17. Model 3. Dependence of $\frac{x}{c}$ upon δ^*/h.

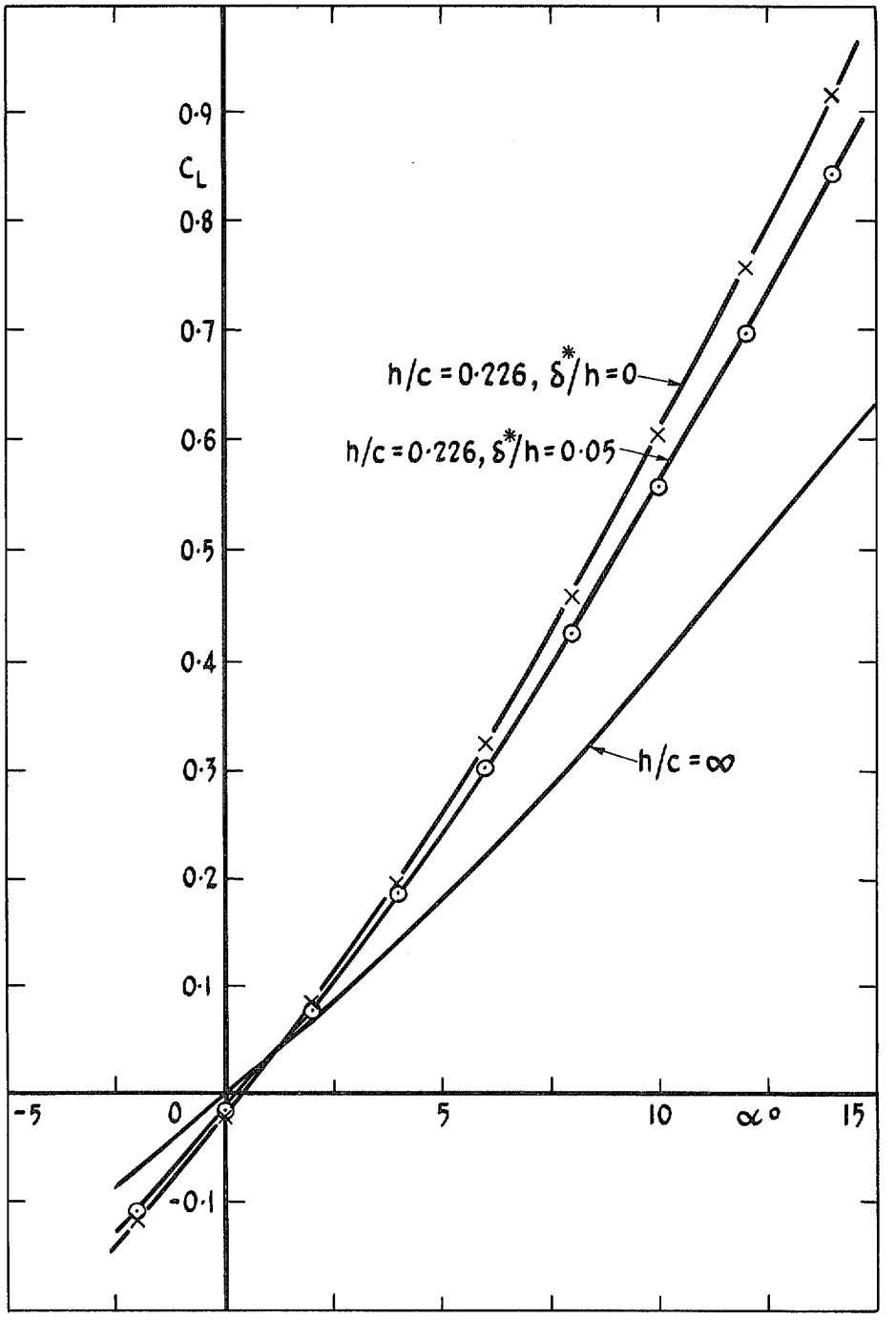

FIG. 18. Model 1. Variation of C_L^* with incidence.

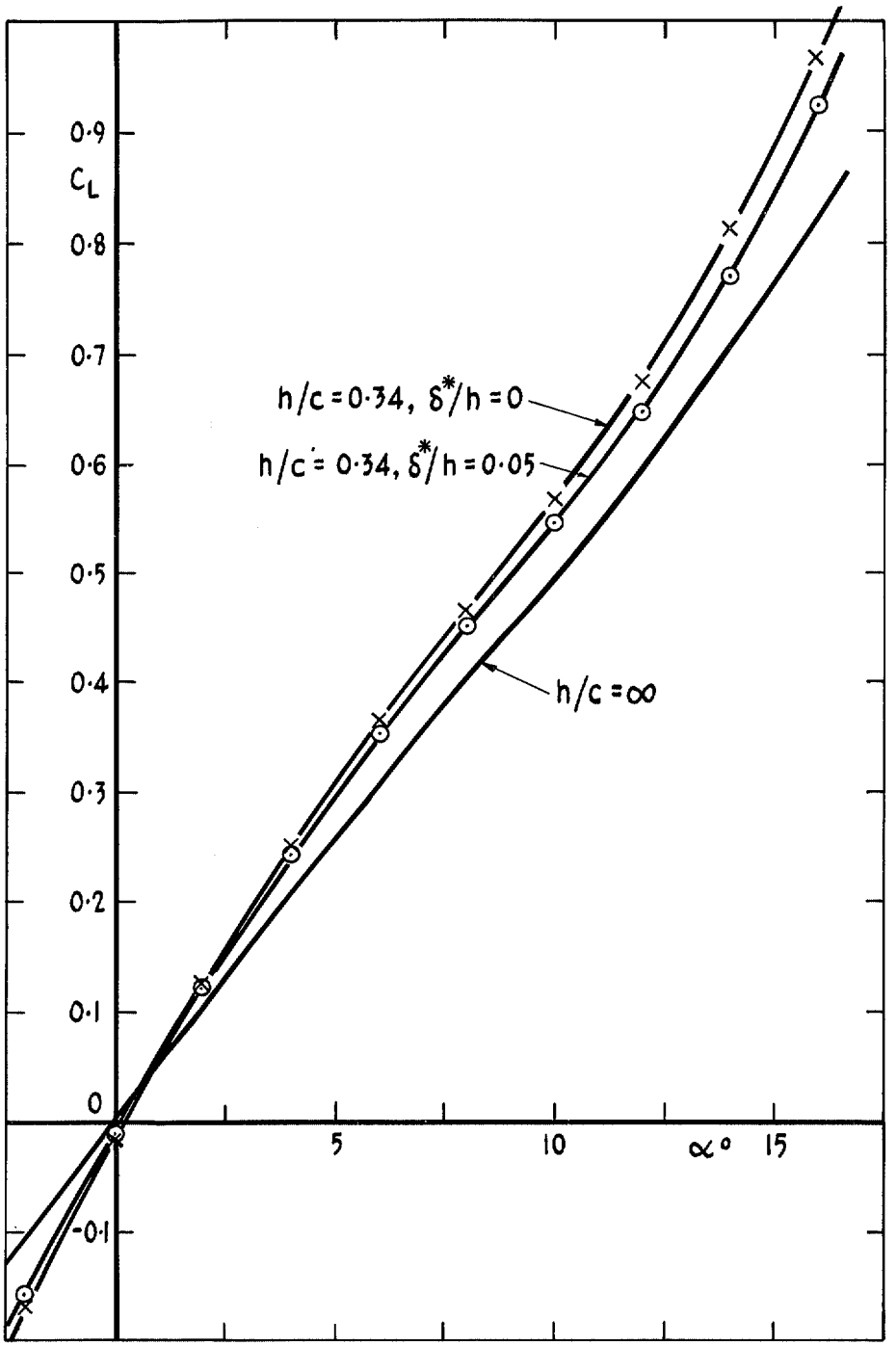

FIG. 19. Model 2. Variation of C_L with incidence.

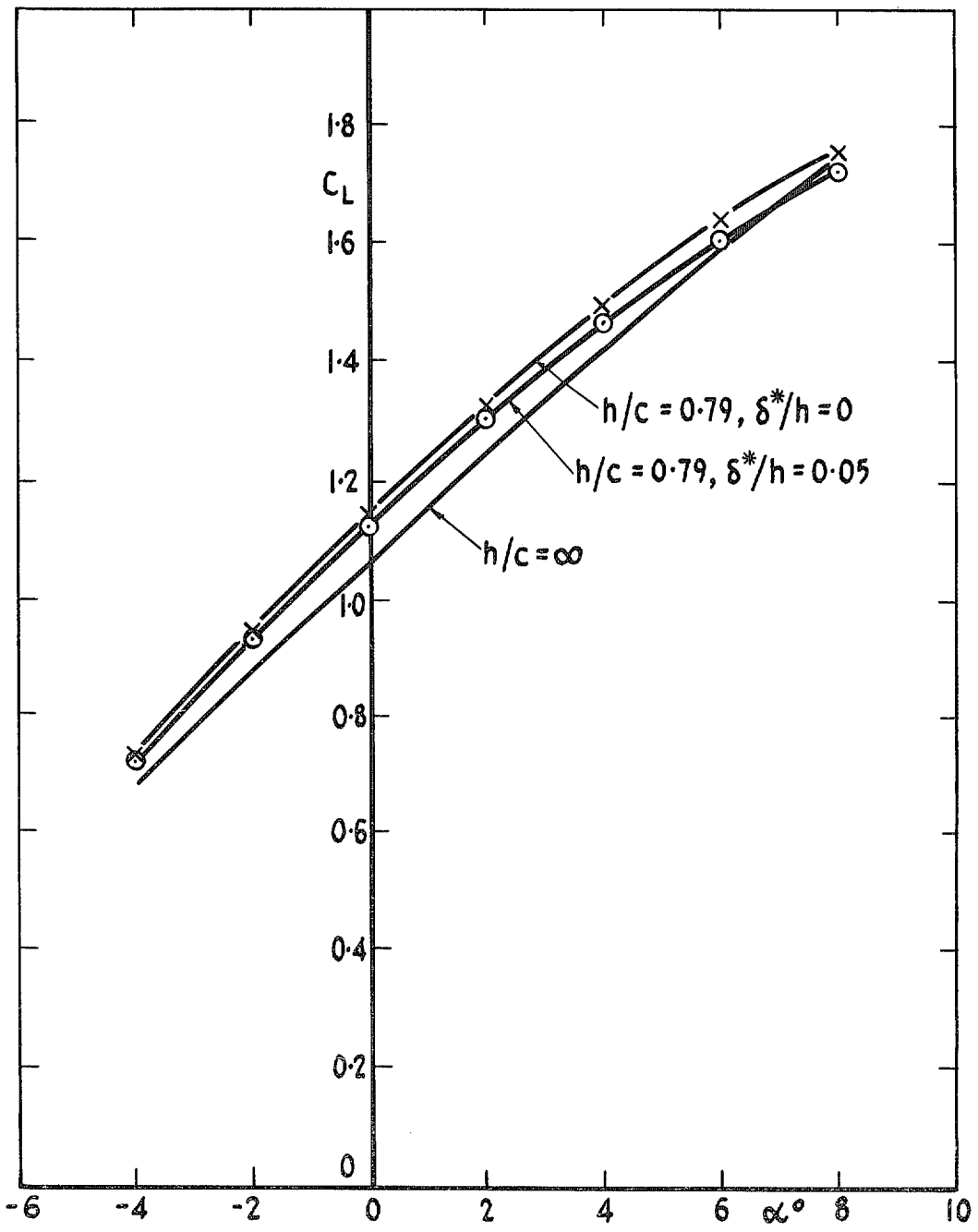

FIG. 20. Model 3. Variation of C_L with incidence.

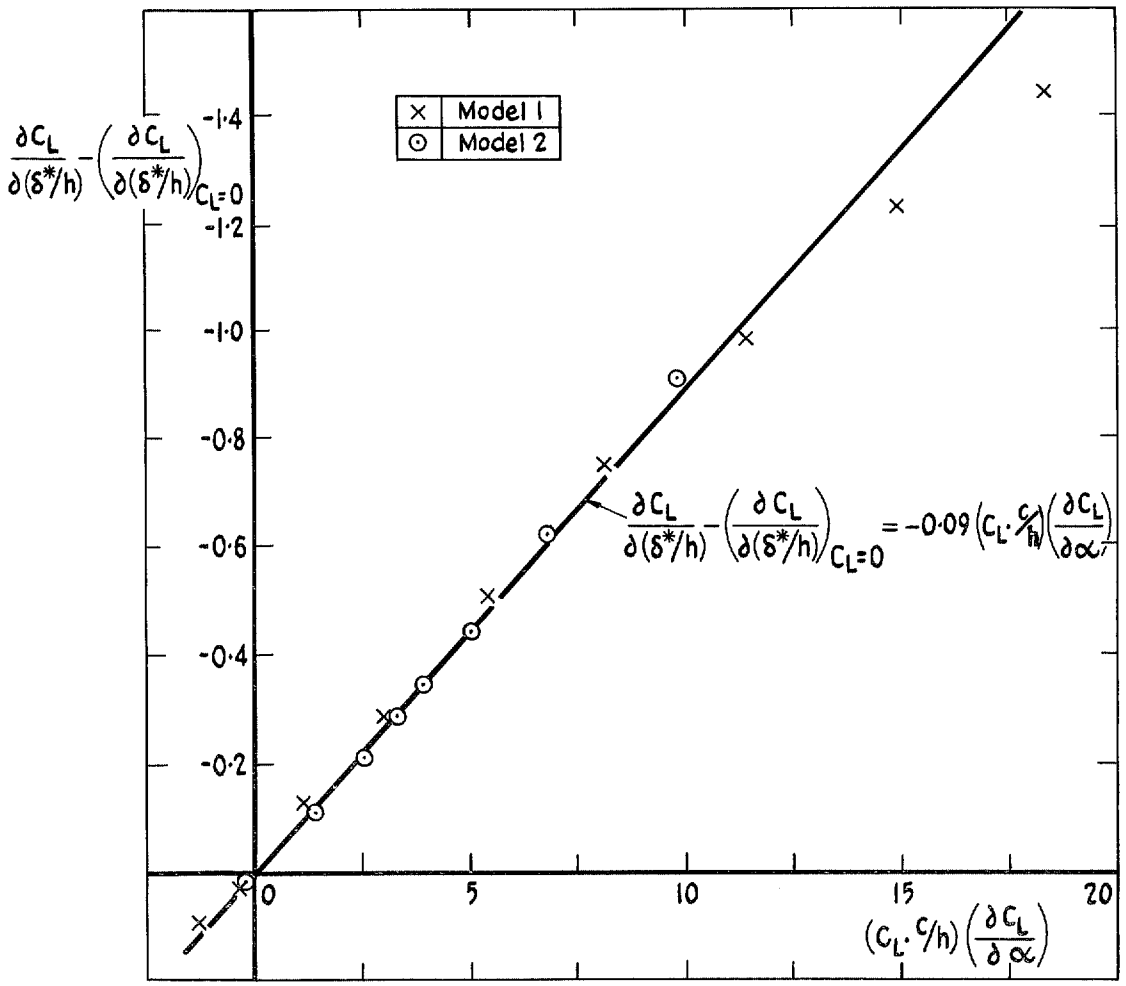

FIG. 21. Models 1 and 2. Correlation of the experimental values of $\partial C_L/\partial(\delta^{*z}h)$ by using equation (5) with $K_1 = -0{\cdot}09$.

Ground board length L	4·267m (14Ft)	3·048m (10Ft)	1·829m (6Ft)
Symbol	×	△	⊙

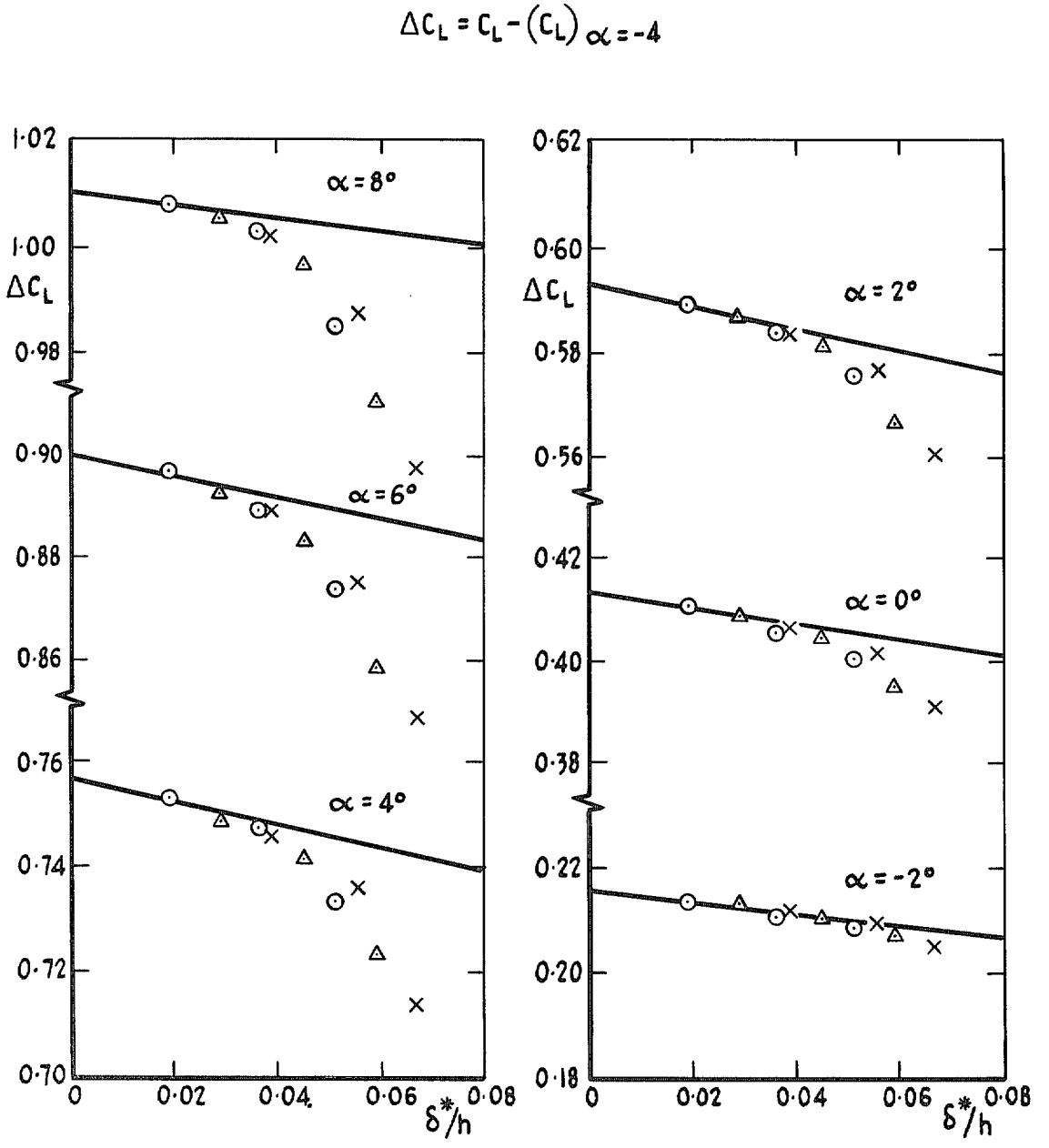

FIG. 22. Model 3. Dependence of ΔC_L upon δ^*/h. Lines shown have gradients given by equation (6) with $K_1 = -0{\cdot}09$.

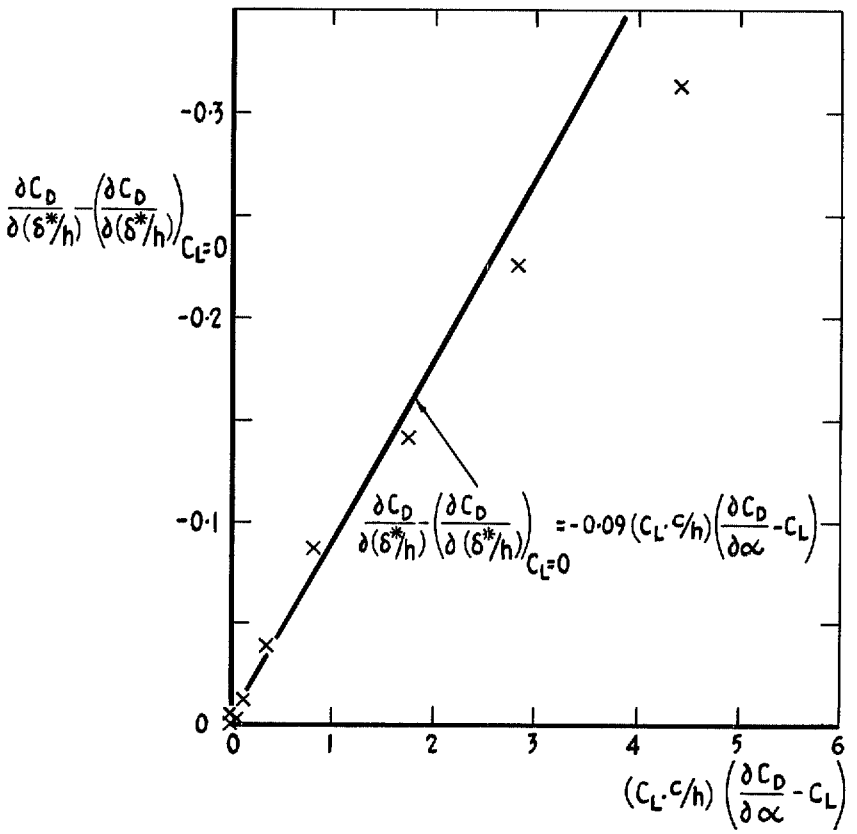

FIG. 23. Model 1. Prediction of $\partial C_D/\partial(\delta^*/h)$ by equation (7), with $K_1 = -0{\cdot}09$, compared with experimental values.

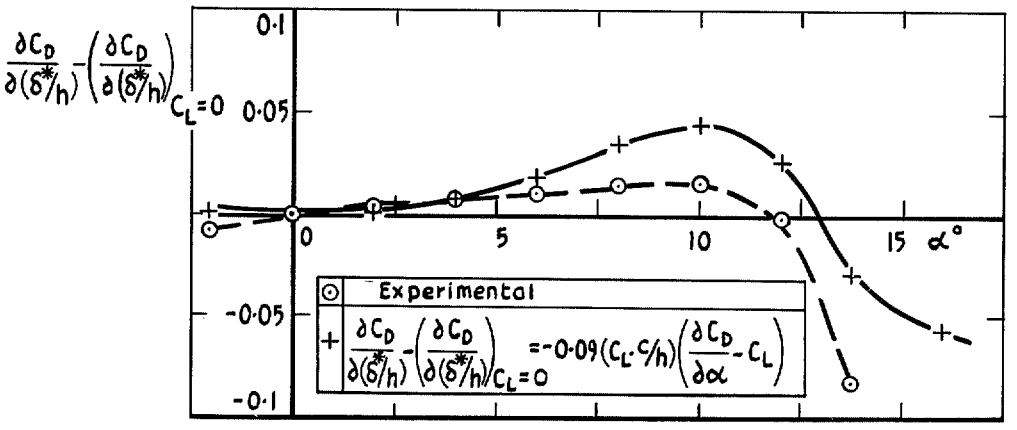

FIG. 24. Model 2. Prediction of $\partial C_D/\partial(\delta^*/h)$ by equation (7), with $K_1 = -0{\cdot}09$, compared with experimental values.

Ground board length L	4·267m (14ft)	3·048m (10ft)	1·829m (6ft)
Symbol	×	△	⊙

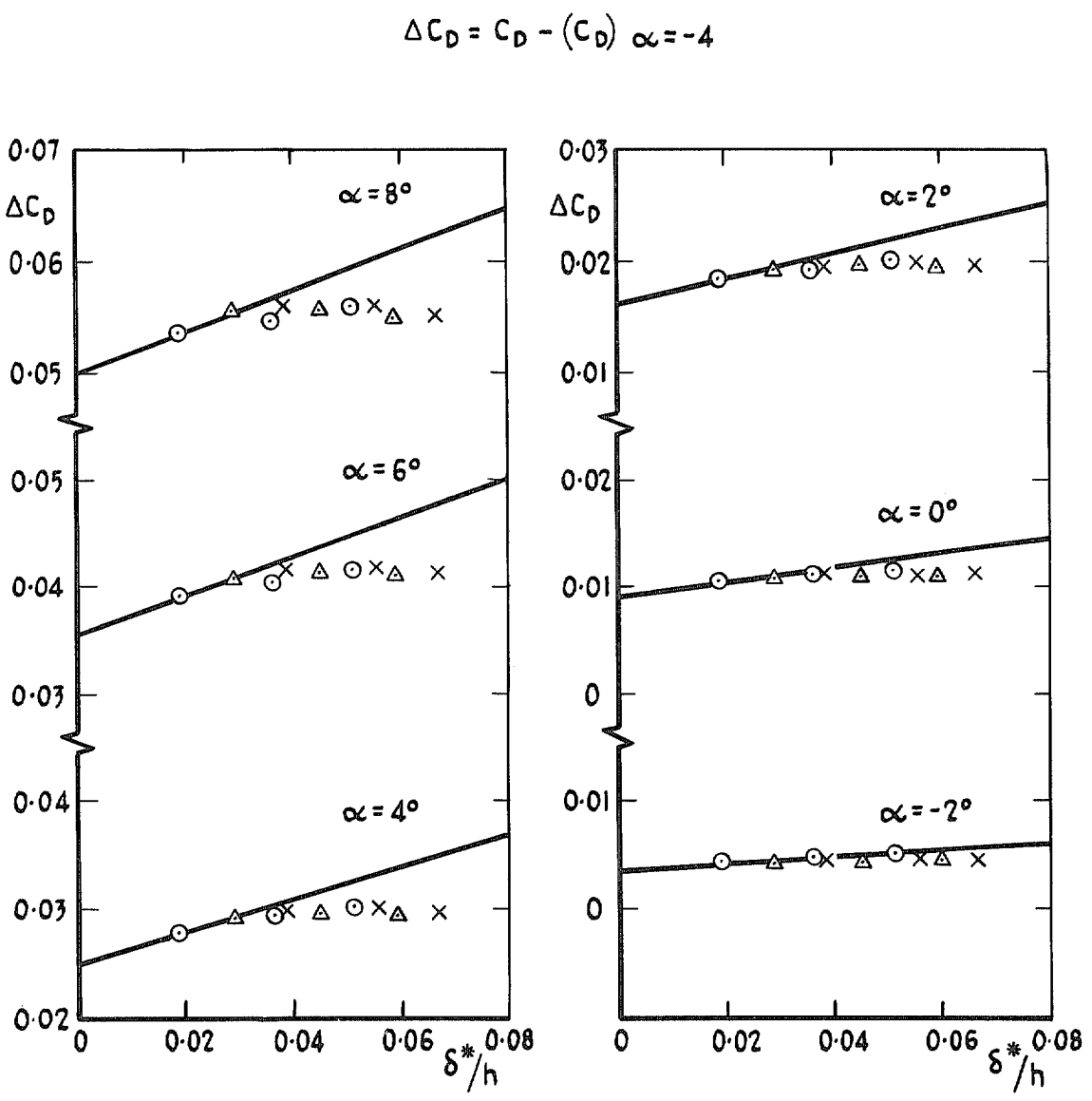

FIG. 25. Model 3. Dependence of ΔC_D upon δ^*/h. Lines shown have gradients given by equation (7) with $K_1 = -0{\cdot}09$.

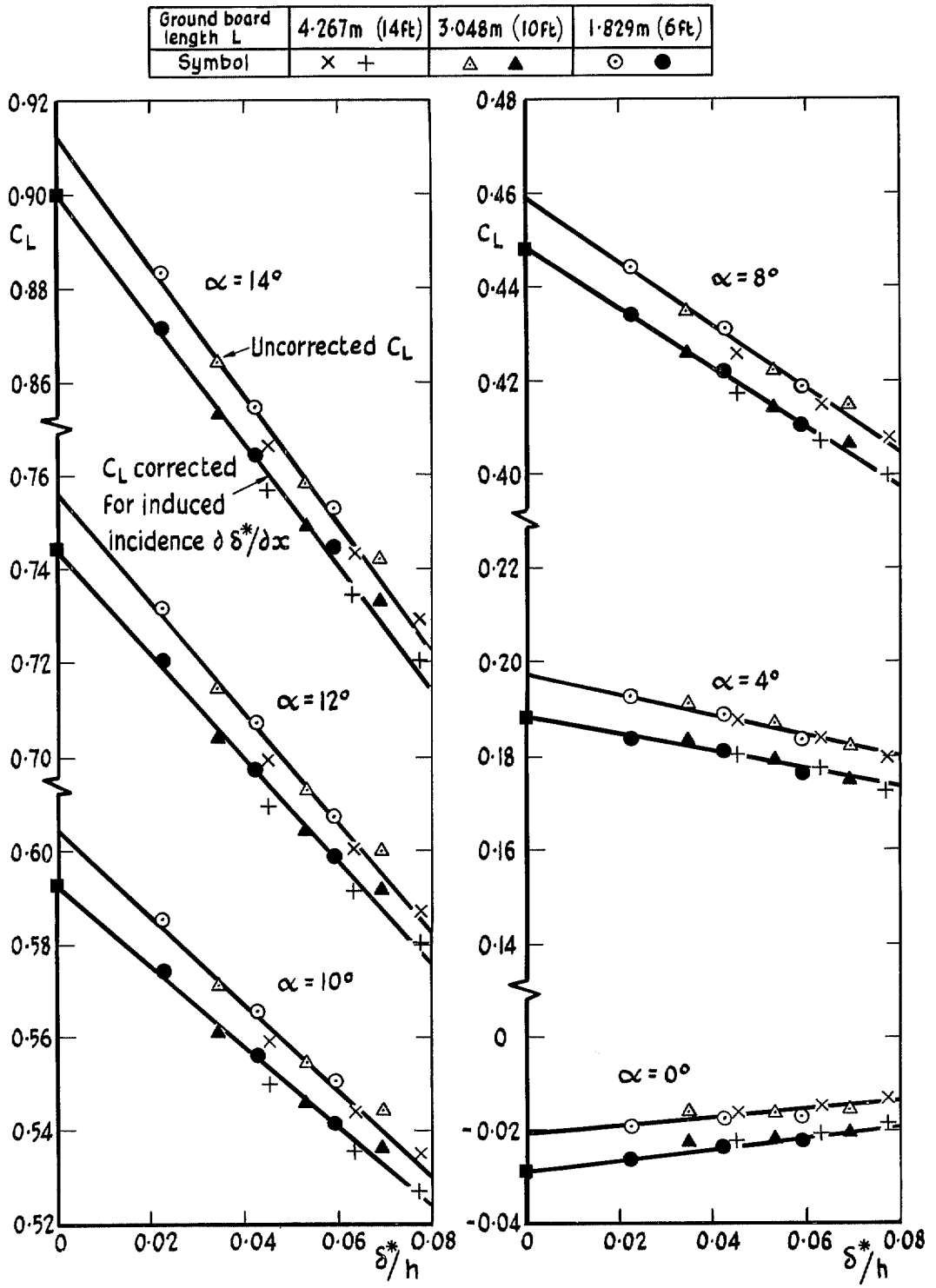

FIG. 26. Model 1. The dependence of C_L upon δ^*/h corrected for an induced incidence of $\partial\delta^*/\partial x$. C_L extrapolated to $\delta^*/h = 0$ and corrected for an induced incidence of 0·16 degrees shown as ■

Ground board length L	4·267m (14ft)	3·048m (10ft)	1·829m (6ft)
Symbol	× +	△ ▲	⊙ ●

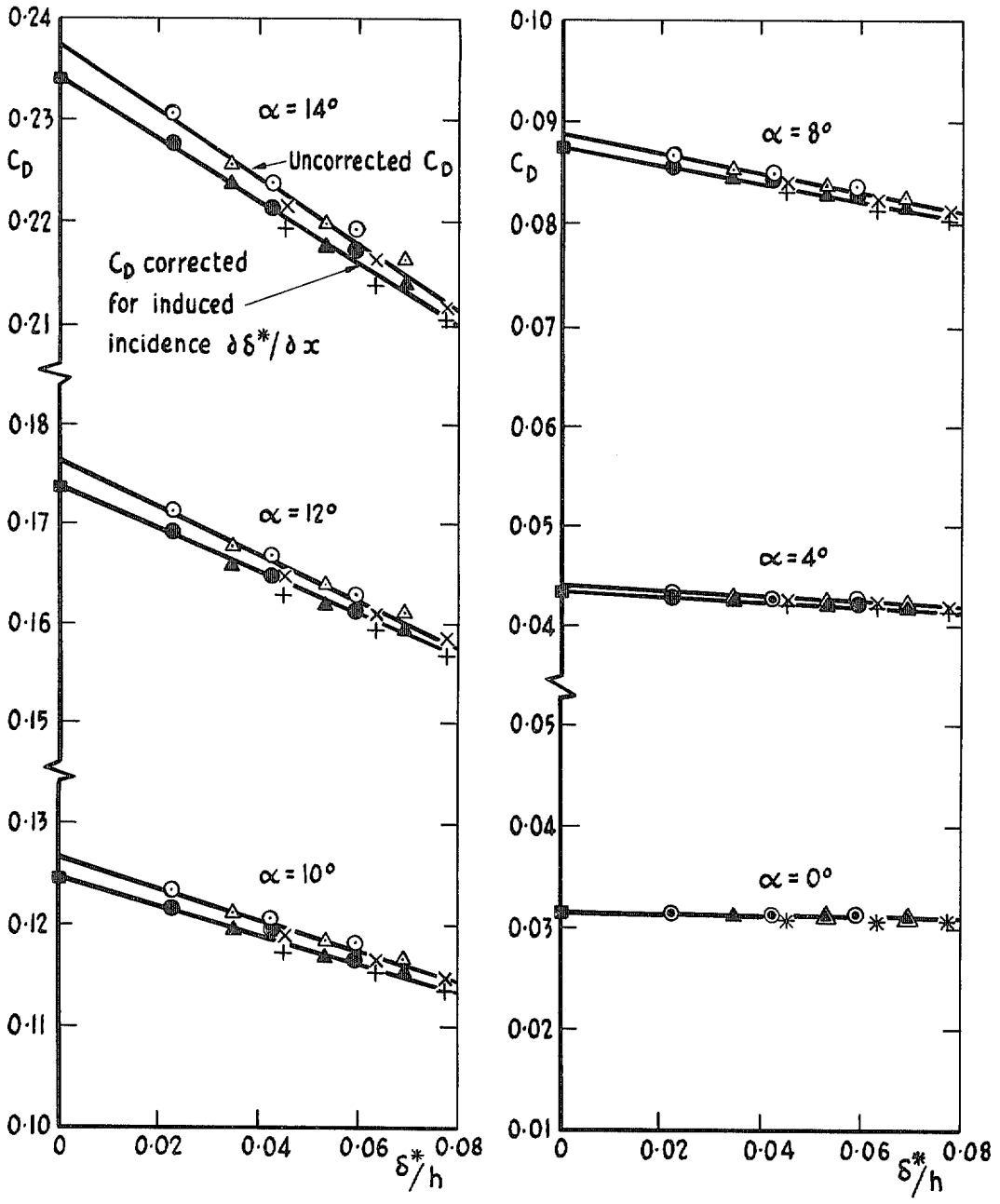

FIG. 27. Model 1. The dependence of C_D upon δ^*/h corrected for an induced incidence of $\partial\delta^*/\partial x$. C_D extrapolated to $\delta^*/h = 0$ and corrected for an induced incidence of 0·16 degrees shown as ■.

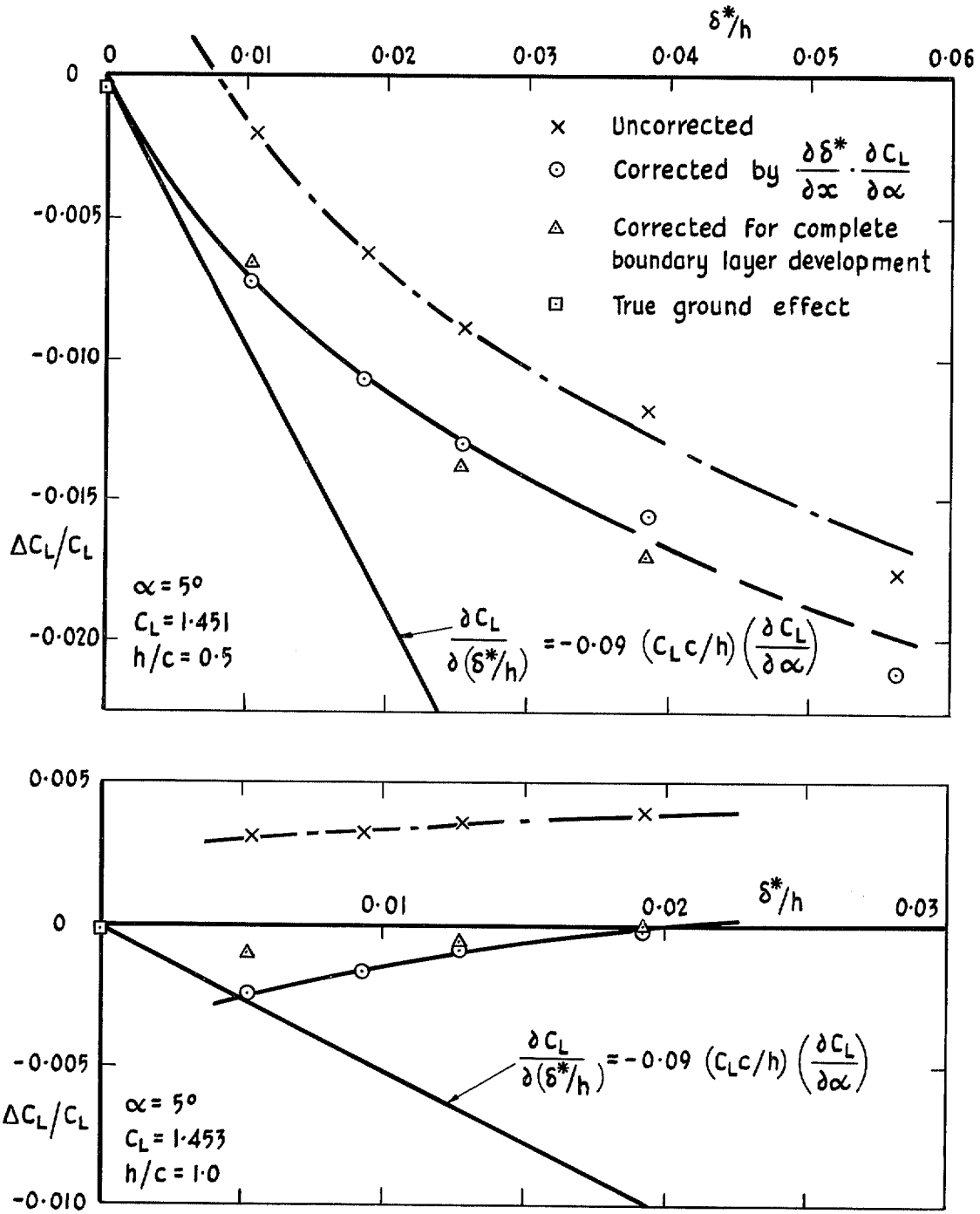

FIG. 28. Computed dependence of C_L upon δ^*/h for a twodimensional aerofoil. $\Delta C_L = C_L - C_L$ (inviscid).

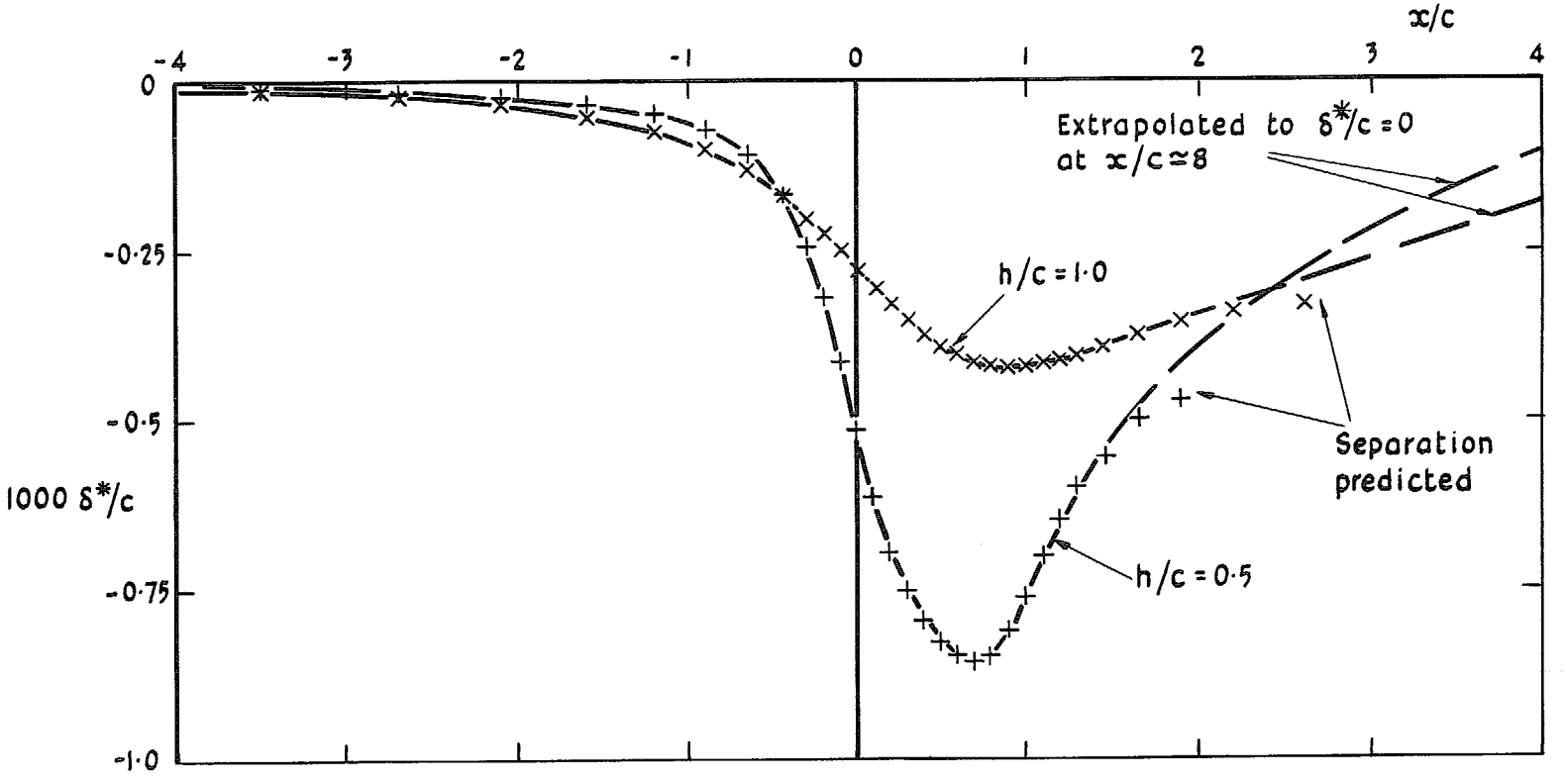

FIG. 29. Development of the true ground boundary layer beneath a twodimensional aerofoil.

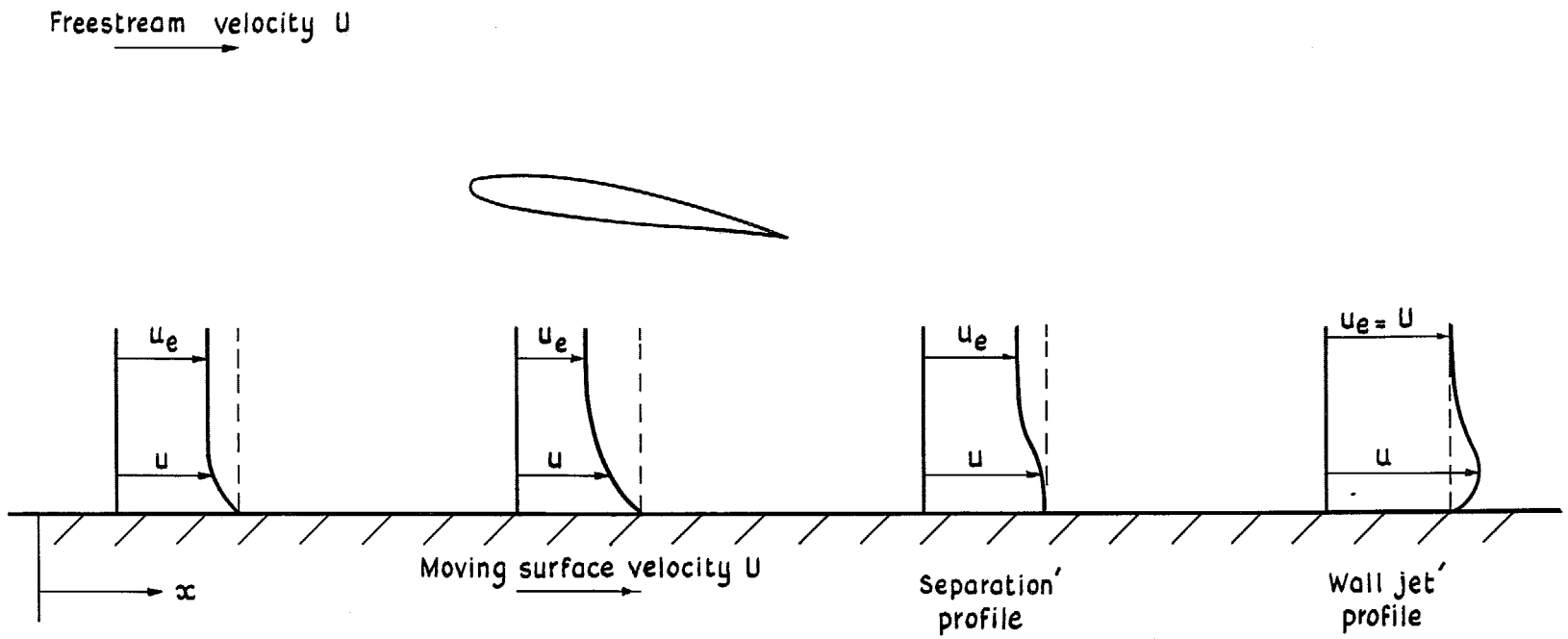

FIG. 30. Sketch of the development of a true-ground boundary layer beneath a twodimensional aerofoil.

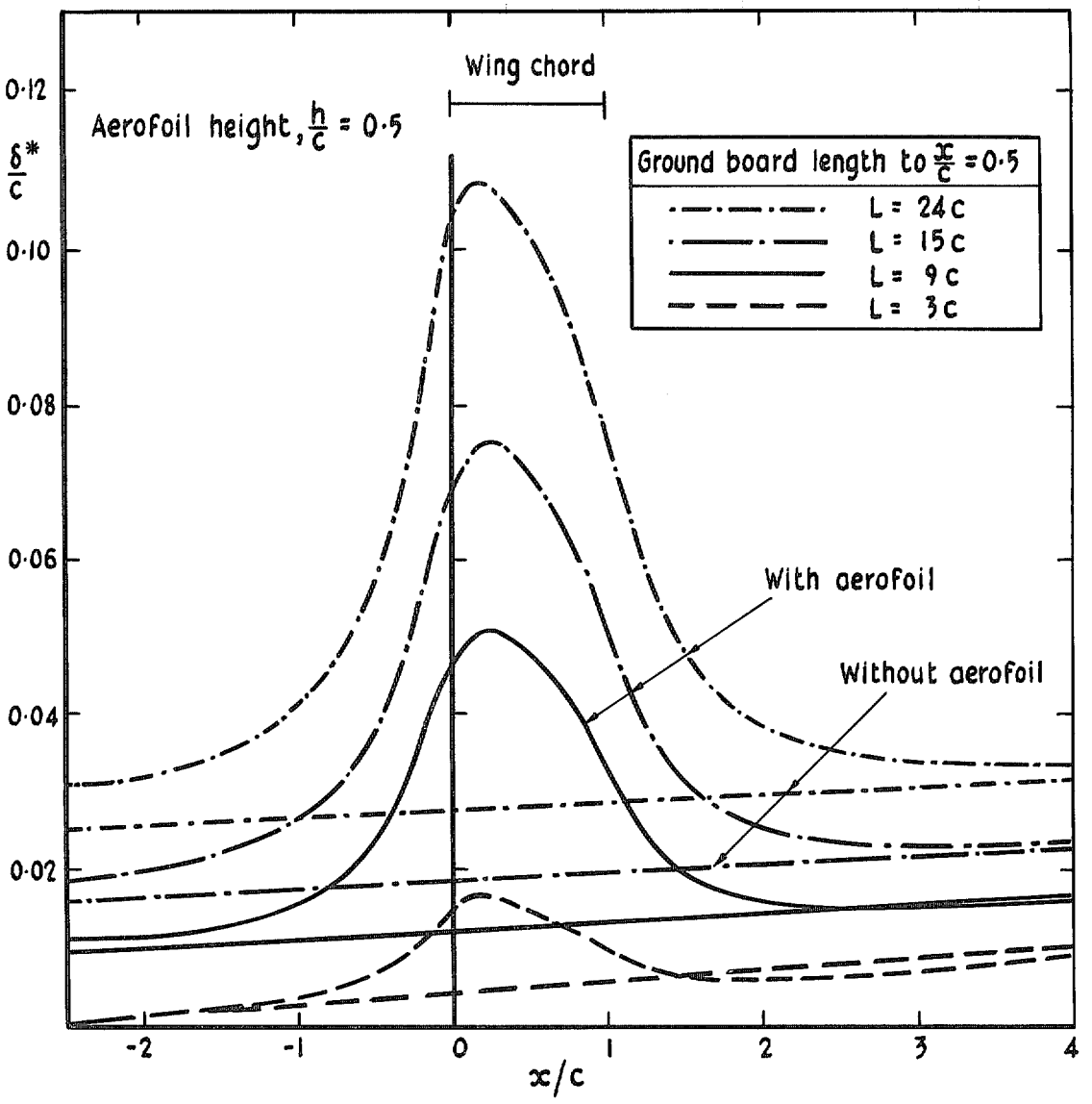

FIG. 31. Variation of the boundary layer displacement thickness along the ground board for various values of L.

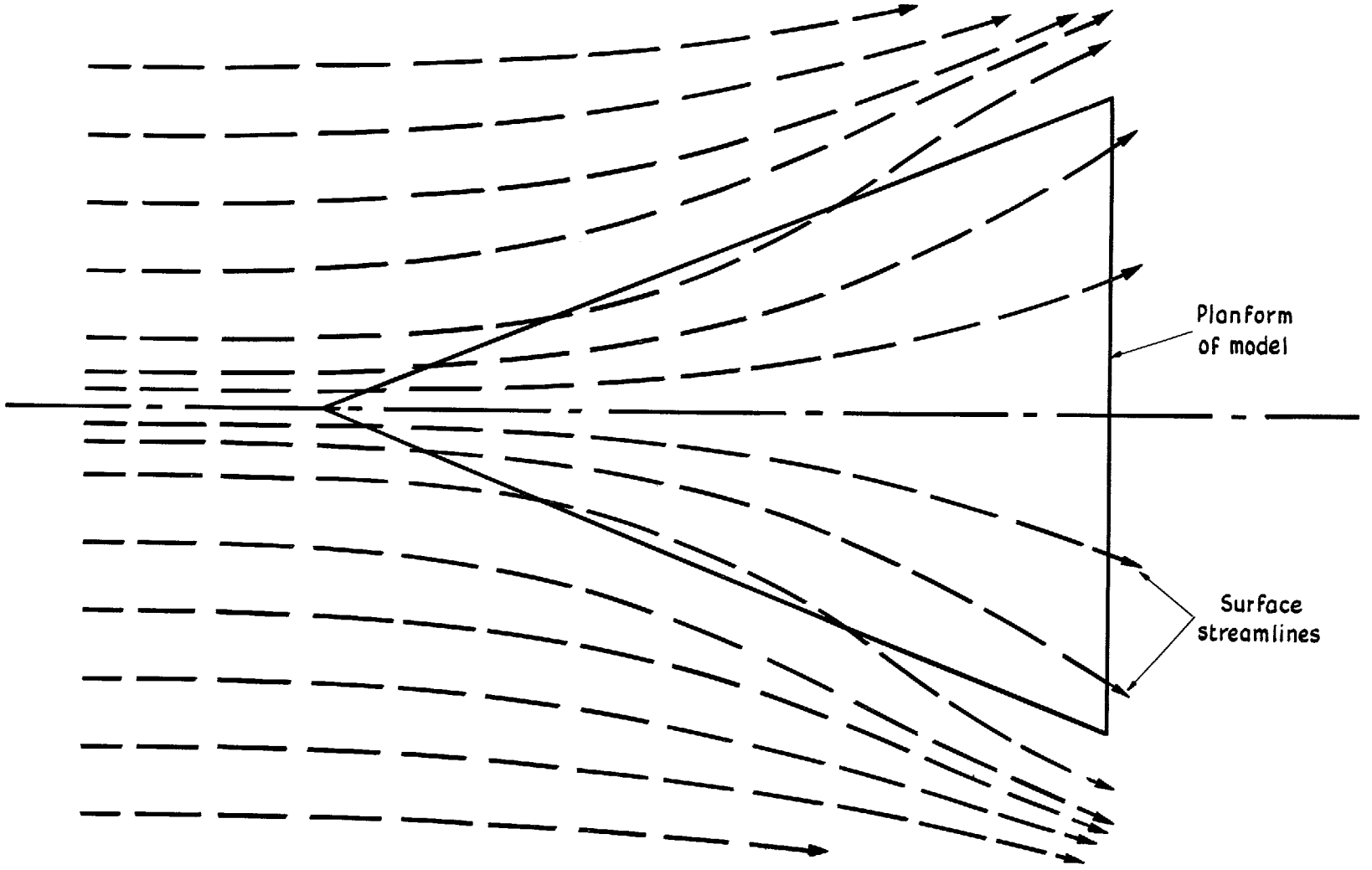

FIG. 32. Pattern of surface flow streamlines on the ground board beneath model 1 obtained from a photograph of the oil flow. Model incidence 8 degrees, nominal velocity 61 m/s (200 ft/s).

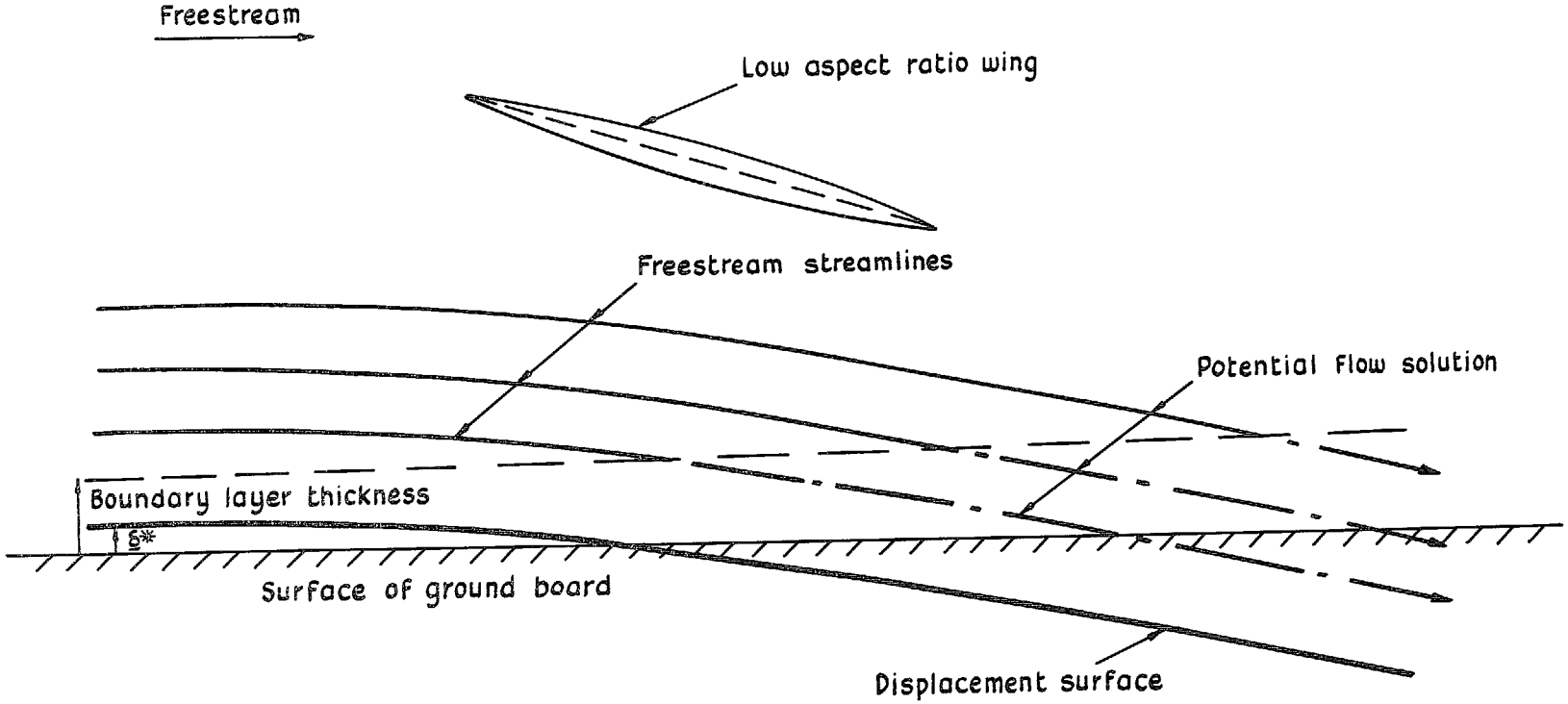

FIG. 33. Sketch of a possible centreline section through the flow about a low aspect ratio wing above a fixed ground board (e.g. as in Fig. 32). Not to scale.

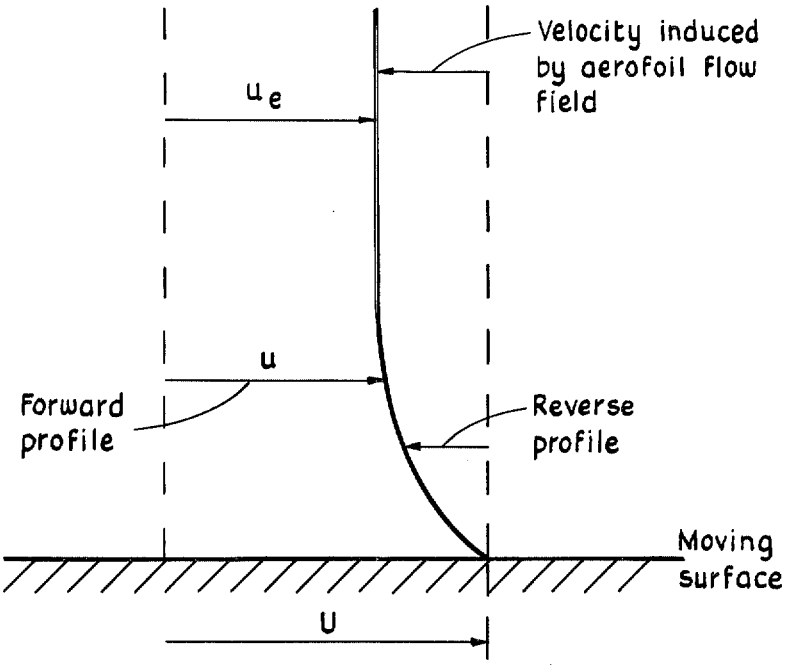

Definitions	Forward profile	Reverse profile
Displacement thickness	$\delta^* = \int \left(1 - \frac{u}{u_e}\right) dy$	$\delta^{*\prime} = \int \left(1 - \left(\frac{U-u}{U-u_e}\right)\right) dy$
Momentum thickness	$\theta = \int \frac{u}{u_e}\left(1 - \frac{u}{u_e}\right) dy$	$\theta' = \int \left(\frac{U-u}{U-u_e}\right)\left(1 - \frac{U-u}{U-u_e}\right) dy$
Shape factor	$H = \delta^*/\theta$	$H' = \delta^{*\prime}/\theta'$
Entrainment parameter	$H_1 = (\delta - \delta^*)/\theta$	$H_1' = (\delta - \delta^{*\prime})/\theta'$

FIG. 34. Typical true-ground boundary layer profile and definitions of various profile parameters.

Printed in Wales for Her Majesty's Stationery Office by Allens Printers (Wales) Limited

Dd. 502110 K.5.

Published by
HER MAJESTY'S STATIONERY OFFICE

To be purchased from
49 High Holborn, London WC1V 6HB
13a Castle Street, Edinburgh EH2 3AR
109 St Mary Street, Cardiff CF1 1JW
Brazennose Street, Manchester M60 8AS
50 Fairfax Street, Bristol BS1 3DE
258 Broad Street, Birmingham B1 2HE
80 Chichester Street, Belfast BT1 4JY
or through booksellers

SBN 11 470489 9